J. Hydrol. Hydromech., 70, 2022, 3, 357–375
https://doi.org/10.2478/johh-2022-0017

sciendo Journal of Hydrology and Hydromechanics Institute of Hydrology SAS

Impact of reconfiguration on the flow downstream of a flexible foliated plant

Marco Maio[1], Gustavo Marini[1*], Nicola Fontana[1], Paola Gualtieri[2], Gerardo Caroppi[2,3]

[1] University of Sannio, Department of Engineering, Piazza Roma 21, 82100, Benevento, Italy.
[2] University of Naples Federico II, Department of Civil, Architectural and Environmental Engineering, Via Claudio 21, 80125, Napoli, Italy.
[3] Aalto University School of Engineering, Department of Built Environment, Tietotie 1E, 02150, Espoo, Finland.
[*] Corresponding author. Tel.: +39 0824 305516. E-mail: gustavo.marini@unisannio.it

Abstract: This paper explores the impacts of reconfiguration and leaf morphology on the flow downstream of a flexible foliated plant. 3D acoustic Doppler velocimetry and particle image velocimetry were used to experimentally investigate the hydrodynamic interaction between a foliated plant and the flow, testing two plants with different leaves morphology under different bulk flow velocities. The model vegetation was representative of riparian vegetation species in terms of plants hydrodynamic behavior and leaf to stem area ratio. To explore the effects of the seasonal variability of vegetation on the flow structure, leafless conditions were tested. Reconfiguration resulted in a decrease of the frontal projected area of the plants up to the 80% relative to the undeformed value. Such changes in plant frontal area markedly affected the spatial distributions of mean velocity and turbulence intensities, altering the local exchanges of momentum. At increasing reconfiguration, the different plant morphology influenced the mean and turbulent wake width. The leafless stem exhibited a rigid behavior, with the flow in the wake being comparable to that downstream of a rigid cylinder. The study revealed that the flexibility-induced reconfiguration of plants can markedly affect the local distribution of flow properties in the wake, potentially affecting transport processes at the scale of the plant and its subparts.

Keywords: Flow-vegetation interaction; Riparian vegetation; Plant reconfiguration; Leaf morphology; Turbulence; Particle image velocimetry; Acoustic Doppler velocimetry.

INTRODUCTION

Vegetation influences the flow characteristics and the ecological functions of many hydro-environments, including rivers, wetlands, and lakes. The additional drag exerted by vegetation increases hydraulic resistance (Nikora et al., 2008; Poggi et al., 2009; Stone and Shen, 2002) with implications on water levels and channel conveyance capacity, also affecting sediment transport (Box et al., 2019; Nepf et al., 1997; Yager and Schmeeckle, 2013). In addition, vegetation influences the bed shear stress and turbulence, affecting the transport of suspended sediments (Tanino and Nepf, 2008; Tinoco and Coco, 2016), playing an important role in the ecological functions for water quality and habitat structure (Gurnell, 2015; Tabacchi et al., 2000). The flow-plants interaction alters the mean and turbulent flow structure. Depending on the plants biomechanical and structural properties, their spatial arrangement and configuration, the presence of plants results in the onset of coherent structures at a variety of scales. In uniformly vegetated channels, the presence of an inflection point on the vertical velocity profile makes the flow susceptible to Kelvin Helmholtz type instabilities and the onset of large-scale vortices (Ackerman et al., 1993; Caroppi and Järvelä, 2022; Zong and Nepf, 2012). Analogously, in partially vegetated channels with emergent vegetation, the velocity gradient in the horizontal plane, similarly to canonical plane mixing layers, generates Kelvin Helmholtz type large-scale vortices dominating the lateral transport of mass and momentum (Caroppi et al., 2020, 2021; White and Nepf, 2008). For patches of vegetation, coherent structures are produced at different scales. Downstream of the patch, a reduction of velocity exists in the wake region, generating periodic vortices, known as von Karman vortex street, enhancing the turbulence intensity and the lateral exchanges of momentum (Biggs et al., 2019; Caroppi et al., 2022). In this case, the von Karman vortex street does not occur directly behind the obstruction but at some distance downstream depending on the patch porosity (Lee et al., 2004). In addition to the large-scale coherent structures, the presence of plants, characterized by a variety of different characteristic lengths (stems diameter, plant height, geometrical characteristics of plant subparts, including the geometrical features of the leaves), results in the generation of a variety of smaller scale coherent structures directly behind the patch (Chen et al., 2012; Zong and Nepf, 2012).

The flow past an individual plant exhibits similarities with the flow past a bluff body. The velocity reduction downstream of the plant causes the periodic vortex shedding in the wake region. Different from the patch scale, the coherent structures downstream a single plant are generated in the vicinity of the obstacle (Boothroyd et al., 2017; Yagci et al., 2010, 2016), with an approximately constant frequency (Nikora et al., 2012 and Siniscalchi and Nikora, 2013b). The effects of coherent structure can be observed across different scales of interaction, from the shear layer scale to the scale of plant subparts (Nikora, 2010).

Understanding the implications of the presence of vegetation on the flow at multiple scales is important for tackling ecological (Nikora et al., 1999) and river management problems (Rowiński et al., 2018), also considering the recent interest in river ecological restoration and the use of NBS for river management (Pugliese et al., 2022). In riverine systems and riparian environments, the presence of different plant species with unique biomechanical and structural properties makes simulating vegetation in models and in experiments a

challenging task. Based on the biomechanical properties, vegetation can be distinguished into rigid (Mossa et al., 2017; Proust et al., 2017; Stoesser et al., 2010; Tanino and Nepf, 2008) and flexible (Järvelä, 2005; Kubrak et al., 2008; Łoboda et al., 2018; Puijalon et al., 2011; Termini, 2015). The hydrodynamics of vegetated channels has conventionally been analyzed simplifying vegetation into arrays of rigid cylinders, for which the frontal projected area, i.e., the area exposed to the flow, is uniform over the depth. Additionally, arrays of rigid cylinders can be described through few characteristic lengths, such as the cylinders diameter and the spacing between the elements. Such representation disregards the flow-influencing biomechanical and morphological features of shrubby and woody riparian vegetation (Caroppi et al., 2021). Vegetation commonly found in riparian areas is characterized by a variety of characteristic lengths, including the stem and branch diameter, the plant height, the leaves geometry, etc. These features can profoundly impact the flow-vegetation interaction and are particularly relevant for the simulation of flow in presence of shrubby and woody vegetation, as occurring in riparian areas. Studies with flexible foliated plants highlighted marked differences in terms of flow features, exchange of mass and momentum, as well as drag forces experienced by plants (King et al., 2012; Weissteiner et al., 2015; Whittaker et al., 2015). Studies of flow-vegetation interaction with natural plants show that properly addressing vegetation features (in terms of morphology, flexibility and spacing) leads to improved description of hydrodynamic processes in vegetated flows (Caroppi and Järvelä, 2022; Nikora et al., 2008; Przyborowski et al., 2019; Sukhodolova and Sukhodolov, 2012).

Under the flow forcing, the plant's leafy and flexible woody parts bend and streamline, reducing the area exposed to the flow; such processes are indicated as reconfiguration (Harder et al., 2004; Vogel, 1989). Vegetation undergoing reconfiguration exhibits a reduction in drag (Boothroyd et al., 2017; Loboda et al., 2018; Miler et al., 2012; Västilä and Järvelä, 2014) that is particularly marked in the presence of leaves. For shrubby and woody vegetation, leaves can contribute up to 90% of the total vegetative drag (Västilä and Järvelä, 2014). For blade-shaped plants, reconfiguration consists mainly in bending, with a consequently decrease of the canopy height. By contrast, for foliated plants, the presence of leaves and branches make reconfiguration a more complex process, involving the bending of the stem, the changing of orientation of plant material, and the streamlining of flexible plant parts under the flow forcing (Caroppi and Järvelä, 2022).

This paper explores the impact of reconfiguration on the mean and turbulent flow features downstream of an isolated flexible foliated plant stand representative of common riparian species. Two plants with leaves of different morphology were used in the flume investigation to study the effects of leaves morphology on the flow. Detailed flow velocity and vegetation frontal area measurements were used to explore the flow-vegetation interaction with a specific focus on the flow spatial variability.

MATERIALS AND METHODS

Experiments were carried out in an 8 m long, 0.4 m wide acrylic-walled recirculating flume at the Laboratory of Hydraulics of University of Naples Federico II. A tailgate located at the flume outlet was adjusted to regulate the water depth, the slope was fixed and equal to 0.48%. The flume bottom was covered by a smooth Plexiglas plate. The occurrence of a subcritical gradually varied flow profile was observed. The isolated plant was positioned at the channel midline at ~5 m from the outlet (~3 m from the inlet), where the flow was fully developed as verified through preliminary measurements. The channel inlet was equipped with a parabolic transition to minimize inlet-related turbulence.

The water depth (H) was equal to 180 mm with the plant stand being just-submerged at all runs. The x, y, and z axes of the coordinate system refers to the longitudinal, lateral, and vertical (normal to the flume bottom) directions, respectively. The coordinate system origin was defined as $x = 0$; $y = 0$ and $z = 0$ at the plant position at the bed; with x positive down-stream, y positive towards the flume left wall, and z positive upwards (Figure 1). In this right-handed Cartesian coordinate system, velocity components were denoted as u, v and w, in the x, y and z directions, respectively.

Description of model vegetation and test runs

Two series of experiments were carried out considering two plants, indicated as P1 and P2, with leaves of different morphology, as shown in Figure 2. For both plants, the stem was 180 mm tall with an average diameter of 4 mm. The stem was made of a steel wire coated with polyethylene with short lateral branches to which leaf clusters could be attached. Each plant consisted of a main stem with 5 lateral branches, each branch was made of short petioles with 4 leaves (Figure 2a and Figure 2c). The leaves of P1 plant were elliptical-shaped with length h of 64 mm and width b equal to 30 mm. P2 plant had leaves of elongated shape, with h = 117 mm and b =15 mm. The ratio h/b (Figure 2) was 2.1 for P1 and 7.8 for P2. The same stem was used for both plants, as to isolate the differences associated with leaf morphology. A third vegetative condition, indicated as leafless condition, with the plant stem without leaves, was analyzed to investigate the effects of seasonal variability of vegetation on the flow.

The vertical distribution of the frontal area $A_d(z)$ of the undeformed plants was measured in dry condition. The images of the plants were acquired through a laser scanner and analyzed by using a MATLAB image processing tool. The total frontal area ${A_d}^{tot} = \int A_d(z)dz$ was equal to 23171 mm^2 and 22765 mm^2 for P1 and P2, respectively, thus presenting comparable total frontal area. The frontal stem area A_S was 570 mm^2, the one-sided leaf area A_L was 1260 mm^2 and 1220 mm^2 for P1 and P2, respectively. The leaf to stem area ratio A_L/A_S was equal to 40 for both P1 and P2, thus falling within the range observed for saplings and seedlings of common riparian species (A_L/A_S = 30 ÷ 70) (Västilä and Järvelä, 2014). The artificial plants were selected based on their biomechanical properties and hydrodynamic behavior, and showed similar reconfiguration behavior as natural floodplain plants (Caroppi et al., 2019, 2021).

In order to assess the effects of reconfiguration on the mean and turbulent flow structure downstream of the plant, experiments were carried out with three different bulk flow velocities: low (LF), medium (MF), and high (HF), with increasing cross-sectional mean velocity U_b (Table 1). U_b was evaluated as Q/BH, with Q being the discharge, B the flume width, and H the normal water depth. The combination of the 3 flow conditions (LF, MF, HF) and the 3 plants (P1, P2 and the leafless stem S) resulted in altogether 9 test runs, as detailed in Table 1.

For each test run, the plant total frontal area ${A_w}^{tot}$ and the vertical distribution of the frontal area ($A_w(z)$) were measured through underwater photography with a Fujifilm FinePix XP 90

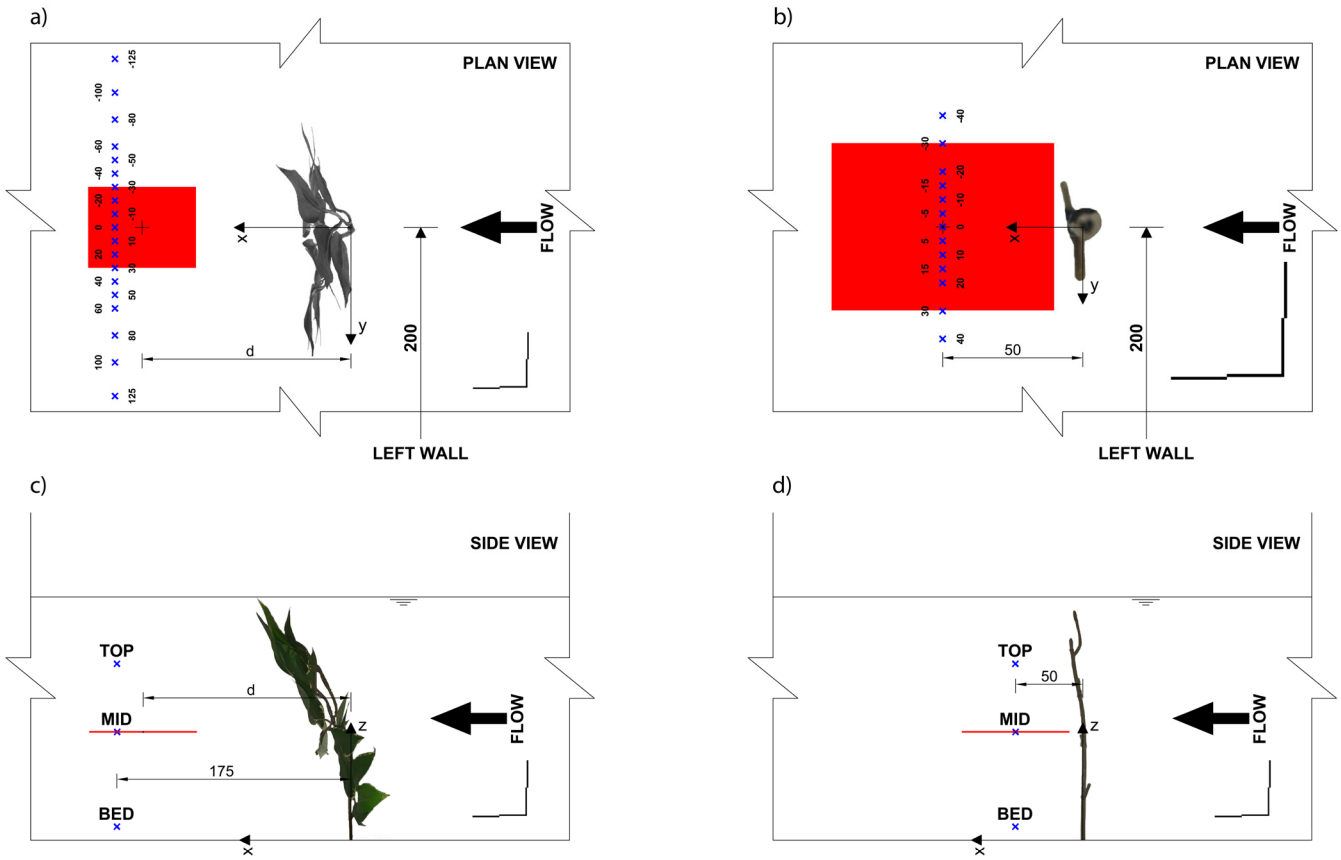

Fig. 1. Plan (a, b) and side (c, d) view of the plant (a and c) and the leafless stem (b and d) within the flume. The blue crosses indicate the positions of the ADV measurement points, the red squares represent the PIV measurement area. *d* indicates the distance between the plant position at the bed and the center of the PIV measurement area (Table 1). Dimensions are in millimeters and black bars correspond to 20 mm.

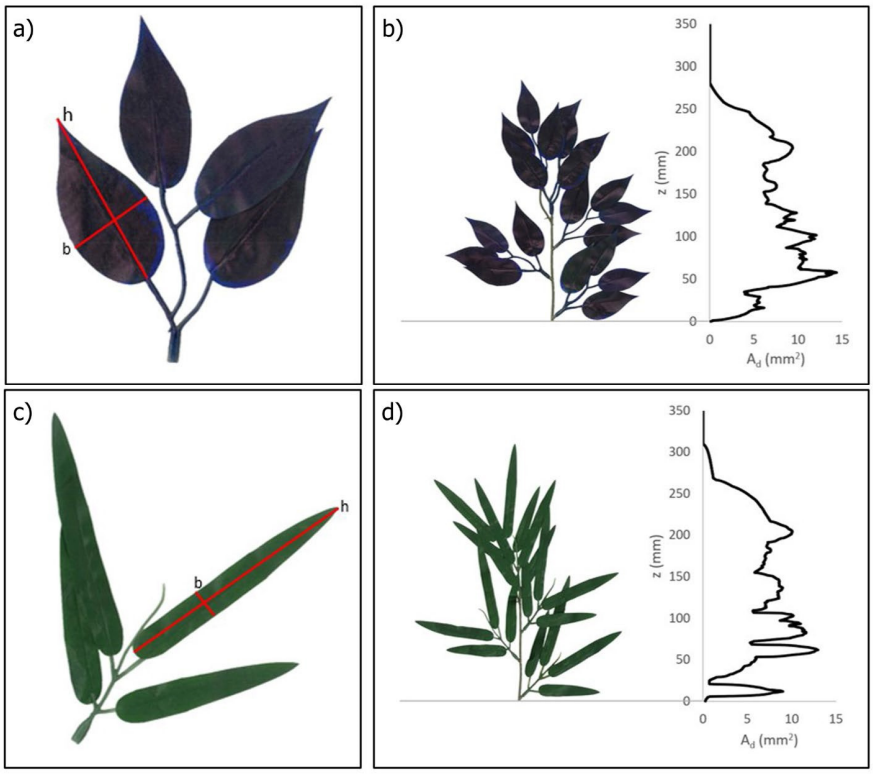

Fig. 2. Leaf clusters of P1 (a) and P2 (c) plant. h and b represent the height and the width of the leaf, respectively. Distribution of the frontal area over the height for P1 (b) and P2 (d) plant as evaluated in dry conditions.

Table 1. Experimental conditions. Q is the flow rate; U_b is the cross sectional velocity; ${A_w}^{tot}$ is the total frontal projected area; l_w is the wake width and d is the longitudinal distance between the plant bed position and the center of the PIV measurement area.

RUN	Plant	Q $(\mathrm{l/s})$	U_b $(\mathrm{m/s})$	${A_w}^{tot}$ $(\mathrm{mm^2})$	l_w (mm)	l_w^{TKE} (mm)	d (mm)
LF_P1	P1	6.3	0.09	13799	127	160	125
LF_P2	P2	6.3	0.09	13269	124	164	125
LF_S	Stem	6.3	0.09	570	10	20	50
MF_P1	P1	15.6	0.22	6914	53	72	150
MF_P2	P2	15.6	0.22	7541	60	92	150
MF_S	Stem	15.6	0.22	570	16	24	50
HF_P1	P1	30.0	0.42	6099	37	53	175
HF_P2	P2	30.0	0.42	7186	48	77	175
HF_S	Stem	30.0	0.42	570	8	20	50

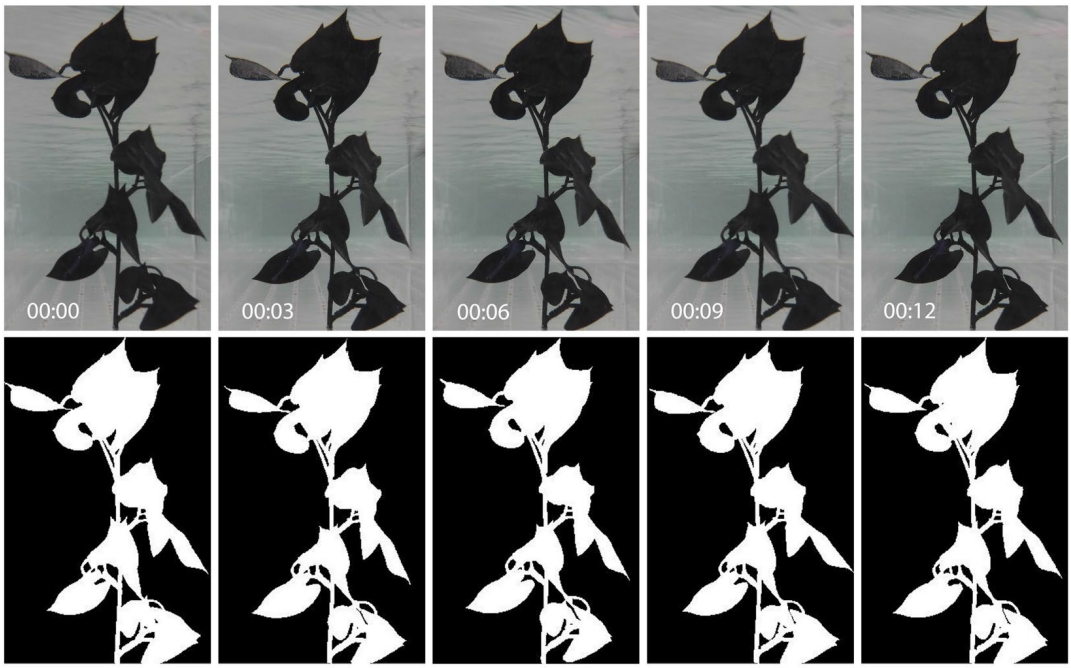

Fig. 3. Selected underwater photos of the P1 plant during the HFP1 test run (upper row) and the corresponding binarized images (lower row) used to measure the frontal projected area. The relative time of acquisition is indicated.

camera and analyzed with a MATLAB image processing tool (Figure 3). For each test run, the frontal area was evaluated as the average value from 10 images acquired every 3s, as to take into account the effects of plant motions on the frontal projected area (Figure 3). The effects of light refraction and perspective distortion were not considered. However, the accuracy of the frontal area measurements was considered sufficient to the purpose of comparing the different test runs of the present study.

Flow field determination

The determination of the flow field was carried out through acoustic Doppler velocimetry (ADV) and particle image velocimetry (PIV). The ADV measurements, performed along three transversal transects situated at different elevations, were used to describe the effect of reconfiguration on the flow field. PIV measurements were used to investigate the flow field with higher resolution, focusing on the spatial variability of the flow at mid-depth.

ADV measurements

3D instantaneous velocity components were measured using a Nortek Vectrino+ ADV with a down-looking probe with accuracy of ±1%. ADV point velocity measurements were carried out 175 mm downstream of the plant (Figure 1), along three horizontal transects at normalized depth $z/H \cong 0.1$, 0.5 and 0.7 (Figure 1), indicated as BED, MID and TOP, respectively. The three elevations were selected to investigate the whole water column. The three elevations were defined considering that the uppermost 50 mm of the water depth could not be sampled with the ADV. For each elevation, velocity was measured along one transversal transect located 175 mm downstream of the plant in the x direction (Figure 1a). Along each transect, velocity was measured at 19 points with variable lateral spacing between 25 mm and 10 mm (Figure 1). For the leafless stem, the transects were located 50 mm downstream of the stem (Figure 1b), each with 13 ADV measurement points. At each ADV measurement point, the velocity was acquired for 150 s at 200 Hz. The raw ADV data

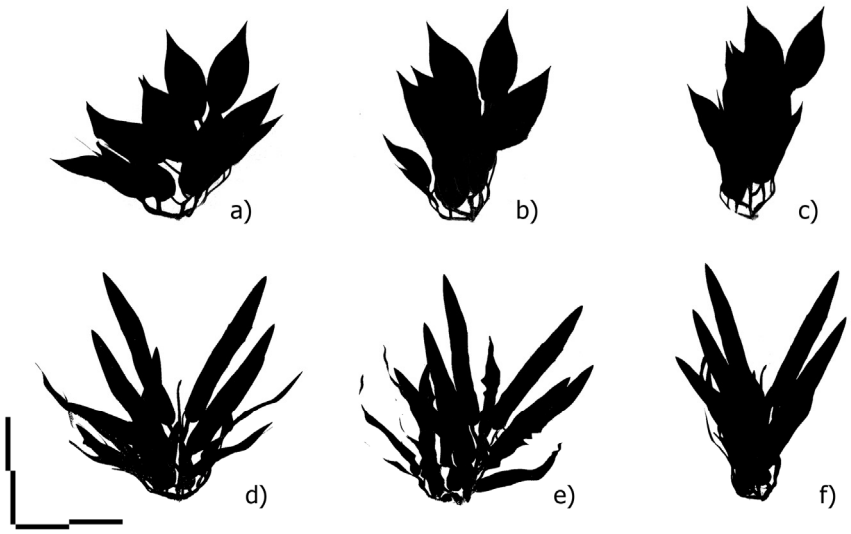

Fig. 4. Binarized images (top view) of plants P1 (a,b, and c) and P2 (d,e, and f) for LF (a,d), MF (b, e) and HF (c,f) flow conditions. Flow direction is from bottom to top. Black bars correspond to 50 mm.

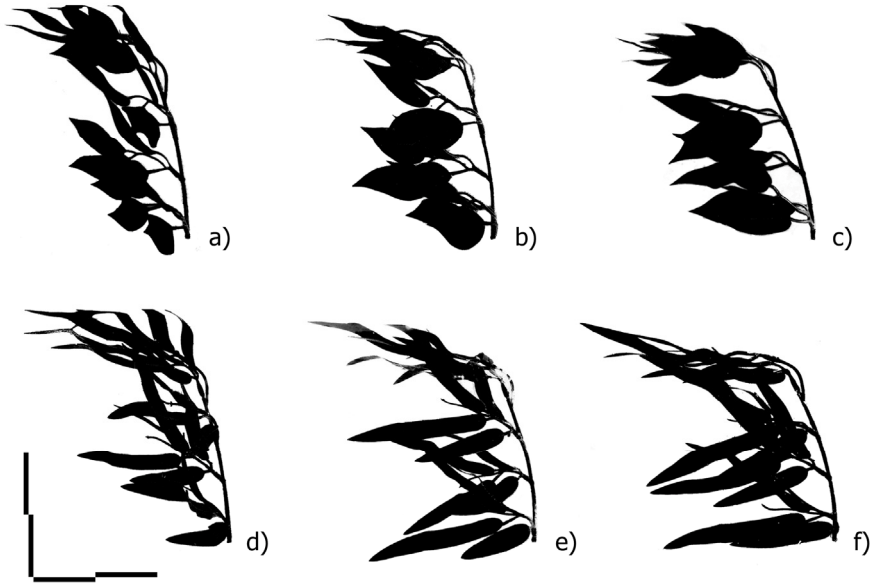

Fig. 5. Binarized images (side view) of plants P1 (a,b, and c) and P2 (d,e, and f) for LF (a,d), MF (b,e) and HF (c,f) flow conditions. Flow direction is from right to left. Black bars correspond to 50 mm.

were pre-filtered discarding values with signal-to-noise ratio and correlation lower than 15 dB and 70%, respectively, and despiked with the Velocity Signal Analyzer software (v1.5.64) (Jesson et al., 2015). Based on the analyses of the effects of the software available spike replacement methods on the velocity statistics, the last good value method was selected (Jesson et al., 2013).

PIV Measurements

The flow filed was further investigated using a DANTEC two-dimensional PIV system. Illumination was provided by a continuum laser RayPower 5000 with 5000 mW output power at a wavelength of 532 nm. The images were acquired through the transparent bottom of the flume, using a high-resolution FlowSense EO VGA camera with 45 mm lens, 640 x 480 px resolution. The images were shot at a rate of 200 frames per second with total sampling time per experiment of 20 s. The total investigated area was 80 x 60 mm^2, with each pixel approximately corresponding to 0.125 mm^2.

The PIV camera was aligned parallel to the bed level below the flume bottom while the laser was placed at the hydraulic left side of the channel. Before running the experiments, the PIV system was calibrated by focusing the camera on a target ruler and the zoom was adjusted to maximize the resolution. The measurement area was parallel to the bed at z = 90 mm and was centered on the axis to the plant (Figure 1). The distance d (along x) between the center of the measurement area and the plant position at the bed (Figure 1) was modified considering the streamlining of plants and was kept constant for cases with the same U_b (Table 1).

The acquisition and post-processing of the PIV images were conducted using Dantec's DynamicStudio v4.10. To obtain particle velocities, the analysis was performed using an interrogation window of 32 x 32 pixels, analyzing the images with the adaptive correlation method with an overlap of 50%.

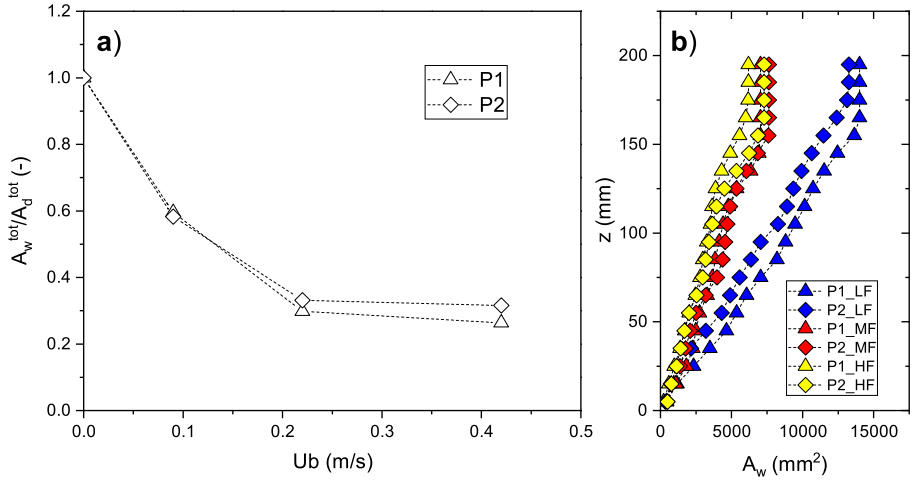

Fig. 6. Dimensionless total frontal area plotted against bulk flow velocity for P1 and P2 (a). Distribution of cumulative area along the height for P1 and P2 for all the tested conditions (b).

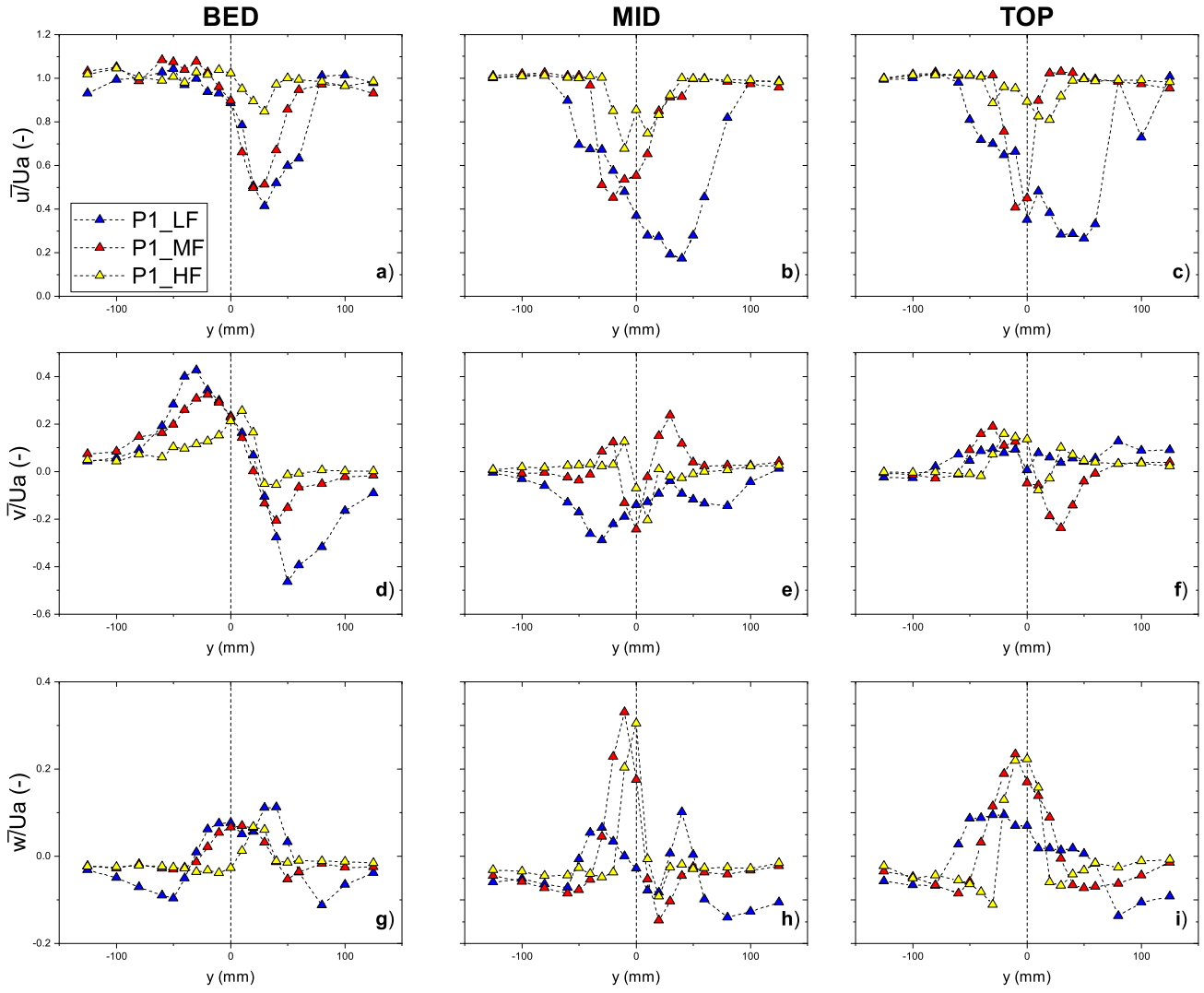

Fig. 7. Time averaged velocity obtained by ADV measurements downstream of P1 normalized with the ambient velocity in the x (a,b,c), y (d,e,f) and z (g,h,i) directions for BED (a,d,g), MID (b,e,h) and TOP (c,f,i) elevations. Each figure shows the results for all flow conditions. The dashed line indicates the position of the plant main stem at the bed.

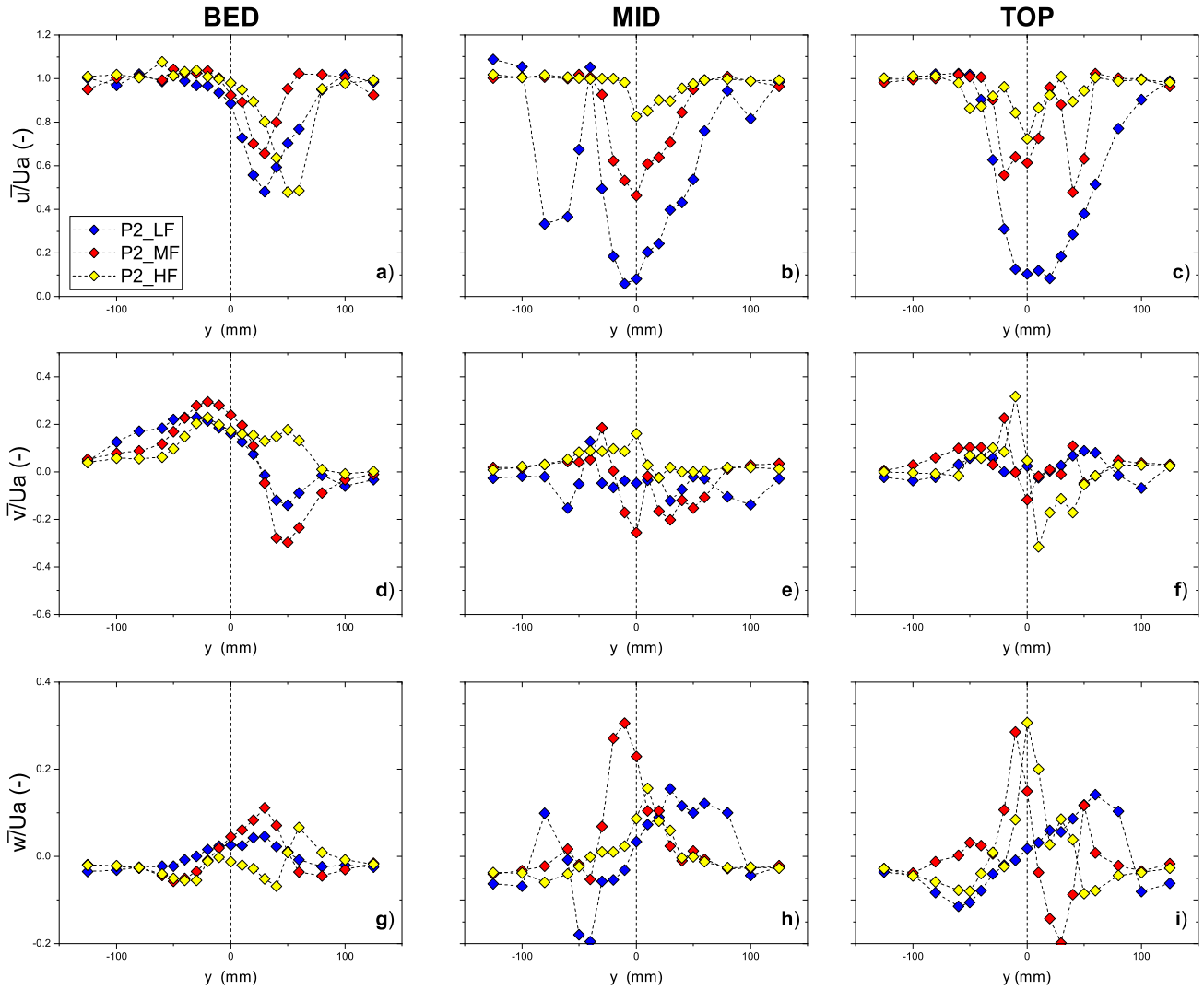

Fig. 8. Time averaged velocity obtained by ADV measurements downstream of P2 normalized with ambient velocity in the x (a,b,c), y (d,e,f) and z (g,h,i) directions for BED (a,d,g), MID (b,e,h) and TOP (c,f,i) elevations. Each figure shows the results for all flow conditions. The dashed line indicates the position of the plant main stem at the bed.

Description of plant reconfiguration and flow field

The magnitude of plant reconfiguration was described with the ratio ${A_w}^{tot}/{A_d}^{tot}$ i.e., the ratio between the total frontal projected area of the reconfigured plant under the flow forcing ${A_w}^{tot}$ and the total frontal projected area of the undeformed plant in dry condition ${A_d}^{tot}$.

The description of the flow field was based on temporally averaged velocity statistics. Each velocity record was decomposed into time-averaged values ($\bar{u}$, $\bar{v}$, $\bar{w}$) and instantaneous fluctuations (u', v', w'). The ADV data were used to evaluate the average velocity $\bar{u}$, $\bar{v}$ and $\bar{w}$ for x, y and z directions, respectively. PIV measurements were used to evaluate $\bar{u}$ and $\bar{v}$.

The turbulent intensity downstream of the plant was described through v_{rms} and u_{rms}, the root mean square of the fluctuating velocity in the y and z directions, respectively. The turbulent kinetic energy per unit mass (TKE) was defined as $TKE = \frac{1}{2}(\overline{u'^2} + \overline{v'^2} + \overline{w'^2})$. The covariances of lateral-longitudinal and lateral-vertical fluctuating velocities cov_{uv} and cov_{vw} were examined to discuss the turbulent momentum fluxes.

The mean and turbulent flow properties were normalized by the local ambient velocity U_a defined as the average velocity in the region lateral to the plant where the flow was not affected by the plant. The mean velocities $\bar{u}$, $\bar{v}$ and $\bar{w}$ were normalized by U_a and the TKE, the root mean square of the fluctuating velocity and covariance were normalized by ${U_a}^2$.

The effects of the plant on the wake geometry were investigated by analyzing the wake width. In this study, we evaluated the wake width both from the transversal profiles of longitudinal velocity (l_w) and the transversal TKE profiles (${l_w}^{TKE}$) (Table 1). l_w was defined as the width of the region where the velocity $\bar{u}$ differed from the local ambient velocity by more than 10%. Analogously, ${l_w}^{TKE}$ was defined as the width of the region where the turbulent kinetic energy differed from the local ambient turbulent kinetic energy by more than 10%. l_w and ${l_w}^{TKE}$ were estimated from the ADV measurements averaging the results from the three transects (BED, MID, and TOP), thus being representative of depth-averaged values.

RESULTS AND DISCUSSION

In this section the results of the experiments are presented first focusing on the effects of the flow forcing on the reconfiguration of the plants and the consequent changes in frontal area.

Successively, the focus is set on the flow field downstream of the plant, as to analyze the effects of reconfiguration and leaves morphology on the mean and turbulent flow field.

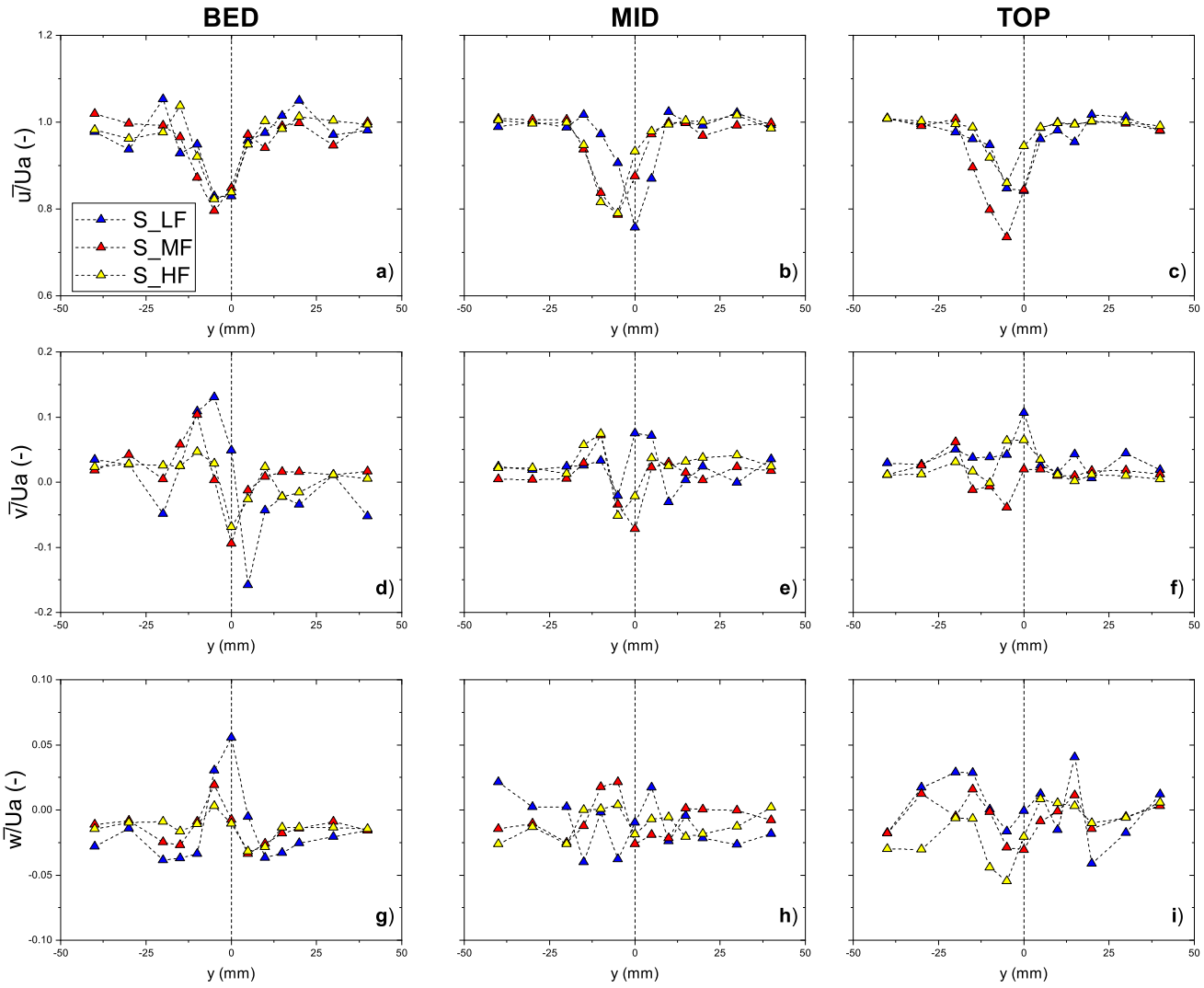

Fig. 9. Time averaged velocity obtained by ADV measurements downstream of the stem normalized with ambient velocity in the x (a,b,c), y (d,e,f) and z (g,h,i) directions for BED (a,d,g), MID (b,e,h) and TOP (c,f,i) elevations. Each figure shows the results for all flow conditions. The dashed line indicates the position of the plant main stem at the bed.

Vegetation reconfiguration

In Figure 4 and Figure 5 the top and side views of P1 and P2 plant under increasing bulk flow velocity are shown. For both plants, with increasing U_b, the stem bent and the leaves and the branches assumed a streamlined position (from a to c, and d to f respectively in Figure 4 and Figure 5). For both P1 and P2 plants, reconfiguration was significant already for the LF conditions. With increasing bulk flow velocity, the streamlining of plant parts increased with a consequent reduction of the area of the plant exposed to the flow. The maximum width of the plants w_p was evaluated from Figure 4 as the distance in the y direction between the two furthest points of the plant. The plant width was used as a measure of the effects of reconfiguration on the plant shape and posture. For the P1 plant, w_p was 219 mm at LF, 158 mm at MF, and 129 mm at HF conditions. Considering that the plant width in dry condition was 276 mm, streamlining resulted in a reduction of the maximum width of 21%, 43%, and 53% at LF, MF and HF, respectively (Table 2). For the P2 plant, the leaves were longer and the maximum width of the plant was 373 mm in dry condition, 251 mm at LF, 220 mm at MF, and 160 mm at HF, corresponding to a reduction of the plant width equal to 33% at LF, 41% at MF and 57% at HF (Table 2).

From the side views of the plant under the flow forcing (Figure 5) it is possible to observe the bending of the plant main stem due to reconfiguration (Table 2). A quantitative information on the plant bending was deduced through the parameter h_p defined as the distance in the x direction between the position of the main stem at the bed (z = 0) and the top (z = 180 mm) (Table 2). With increasing bulk flow velocity, more pronounced bending resulted for both plants, with small differences in bending observed between P1 and P2. At LF and MF, h_p was measured from the acquired side view images (Figure 6) as the distance in x direction between the stem position at bed (z = 0) and the stem position at top (z = 180 mm). Comparing the measurements for the plants, for the LF and MF condition P2 showed greater deflection than P1: indeed h_p at LF and MF was 20 mm and 22 mm for P1 and P2, respectively. At HF, P1 showed a greater bending relative to P2, with h_p = 34 mm and 29 mm for P1 and P2, respectively.

The frontal projected area was measured at each run to provide a quantitative measurement of the overall level of reconfiguration of the plants. The increasing bulk flow velocity from LF to

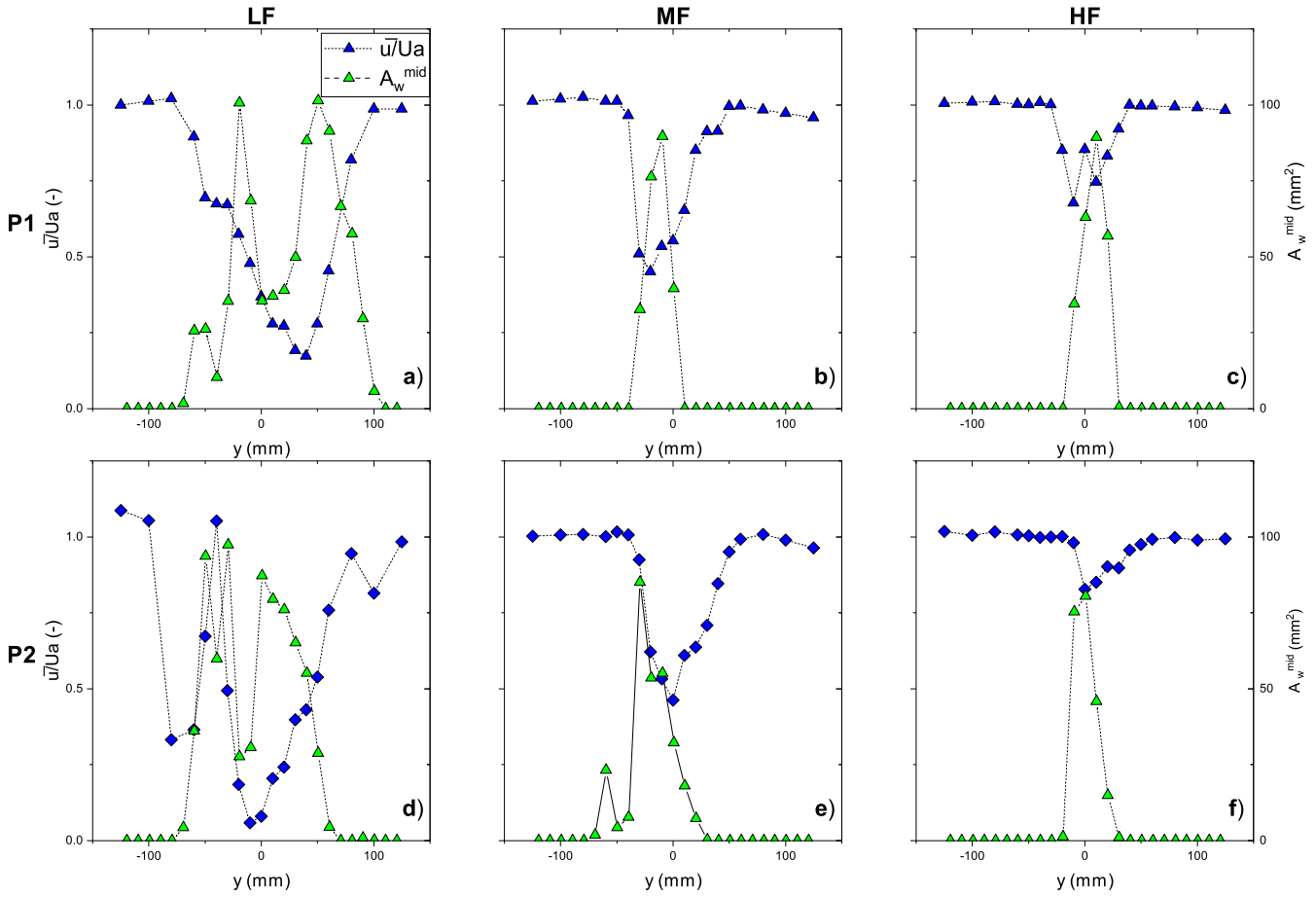

Fig. 10. Normalized time averaged velocity in the $\boldsymbol{x}$ direction and frontal area of P1 (a,b,c) and P2 (d,e,f), at mid-depth for LF (a,d), MF (b,e) and HF (c,f).

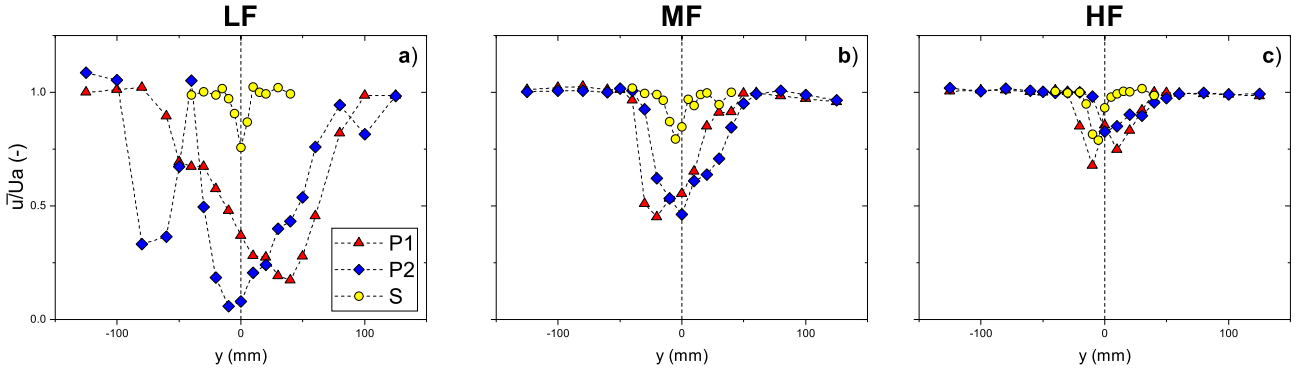

Fig. 11. Normalized time averaged velocity in the $\boldsymbol{x}$ direction at 90 mm for P1, P2 and S; and for LF (a), MF (b) and HF (c). The dashed line indicates the position of the plant main stem at the bed.

Table 2. Reconfiguration parameter. w_p is the maximum width; h_p is the bending of the stem; and Δw_p is the reduction of w_p relative to the dry condition.

RUN	$\boldsymbol{w_p}$ **(mm)**	$\boldsymbol{h_p}$ **(mm)**	$\Delta \boldsymbol{w_p}$ (%)
DRY_P1	276	0	/
DRY_P2	373	0	/
LF_P1	219	20	21
LF_P2	251	22	33
MF_P1	158	20	43
MF_P2	220	22	41
HF_P1	129	34	53
HF_P2	160	29	57

HF resulted in a reduction of the total frontal area for both plants, independently from the morphology of the leaves. In Figure 6a, the total frontal projected area ${A_w}^{tot}$ normalized by ${A_d}^{tot}$ is plotted against the bulk flow velocity U_b. A marked decrease was observed for ${A_w}^{tot}/{A_d}^{tot}$ for LF and MF conditions, with a reduction of the total frontal area of 80% at the highest bulk flow velocity. These observations are in agreement with the results obtained from experiments with real plants (Jalonen and Järvelä, 2014) and with willow twigs (Aberle and Järvelä, 2013).

Figure 6b reports the vertical distributions of the cumulative frontal projected area ($A_w(z)$) for both P1 and P2. No significant differences in the vertical distributions of the frontal area and the total frontal area were observed between both plants. Based on the results in Figure 6b, the highest variation in area along

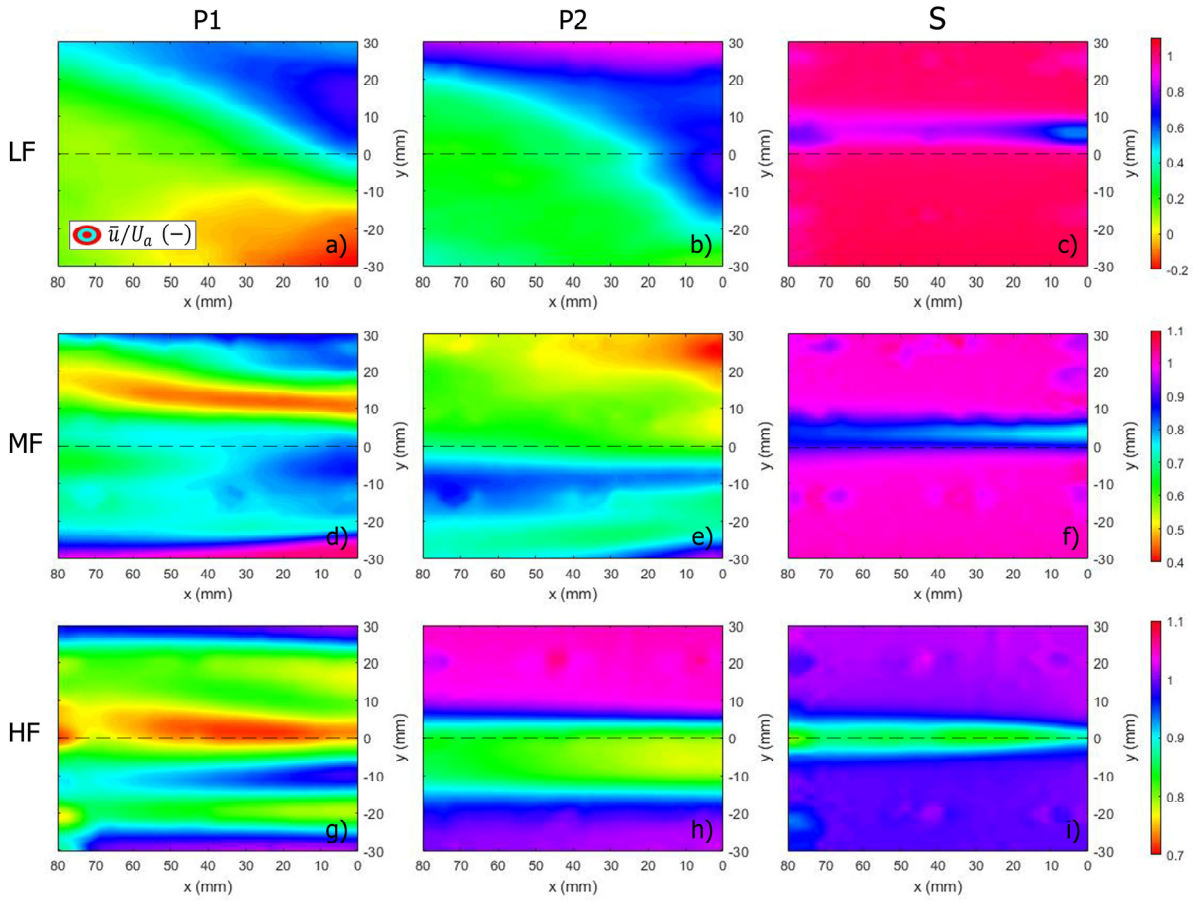

Fig. 12. Normalized time averaged velocity in the $\boldsymbol{x}$ direction obtained by PIV measurements at 90 mm from the bottom in a plan of 80 mm x 60 mm, for P1 (a,d,g), P2 (b,e,h) and S (c,f,i); for LF (a,b,c), MF (d,e,f) and HF (g,h,i). Flow direction is from right to left. The dashed line indicates the position of the plant main stem at the bed.

the height ($A_w(z)$) was measured between LF and MF. Indeed, the total frontal area at LF was 14006 mm^2 and 13261 mm^2 for P1 and P2 respectively while at increasing U_b, at MF it decreased up to 7035 mm^2 and 7629 mm^2 for P1 and P2 respectively. Lower differences were observed between MF and HF for which the measured frontal projected area was 6194 mm^2 and 7295 mm^2 for P1 and P2.

For the tests with the leafless plant, a rigid behavior was observed for the stem, with limited bending. For the leafless stem the stem frontal area remained constant among the runs.

Mean flow field

The flow field downstream of the plants P1 and P2 and the stem S is described in the following sections by focusing firstly on the effects of reconfiguration and secondly on the effects of leaves morphology.

Effects of reconfiguration

The effects of reconfiguration for each plant were investigated by comparing the lateral distributions of mean velocity evaluated at the three elevations (BED, MID and TOP) under the three different bulk flow velocities. Figure 7 reports the dimensionless time-averaged velocity ($\bar{u}/U_a$; $\bar{v}/U_a$; $\bar{w}/U_a$) for P1 for all the test cases.

For all the tests, the normalized streamwise velocity $\bar{u}/U_a$ downstream of the plant was lower than the ambient velocity, exhibiting a reduction in velocity as typically observed in the wake of bluff bodies (Tritton, 1977). The inflection on the velocity profile has been observed in analogous studies with rigid cylinder and porous obstructions (Shadaram et al., 2008). The presence of the inflection point makes the flow susceptible to the instability of von Kármán (Zong and Nepf, 2012).

The differences in the velocity reduction downstream of the plant along the vertical direction (i.e., between the BED, MID and TOP transects) is attributed to the heterogeneous vertical distribution of the plant frontal area. Moreover, the changes in the spatial distribution of the velocity and of the magnitude of the velocity reduction can be ascribed to the increasing bulk flow velocity and plant reconfiguration. Specifically, the wake width (l_w) measurements at LF showed an average of 127 mm, with the smallest l_w at BED (75 mm) and the greatest at MID (160 mm). Due to reconfiguration, the wake width showed a marked decrease with increasing bulk flow velocity: for the highest bulk flow velocity, l_w was on average 37 mm, with the greatest reduction at MID (from 160 mm at LF to 50 mm at HF).

The presence of vegetation generates a “dead zone” downstream of the plant (Yagci et al., 2010), i.e., a zone with lower magnitude of streamwise velocity. This was particularly marked at LF for which the magnitude of normalized velocity decreased by up to 70% relative to the ambient velocity value,

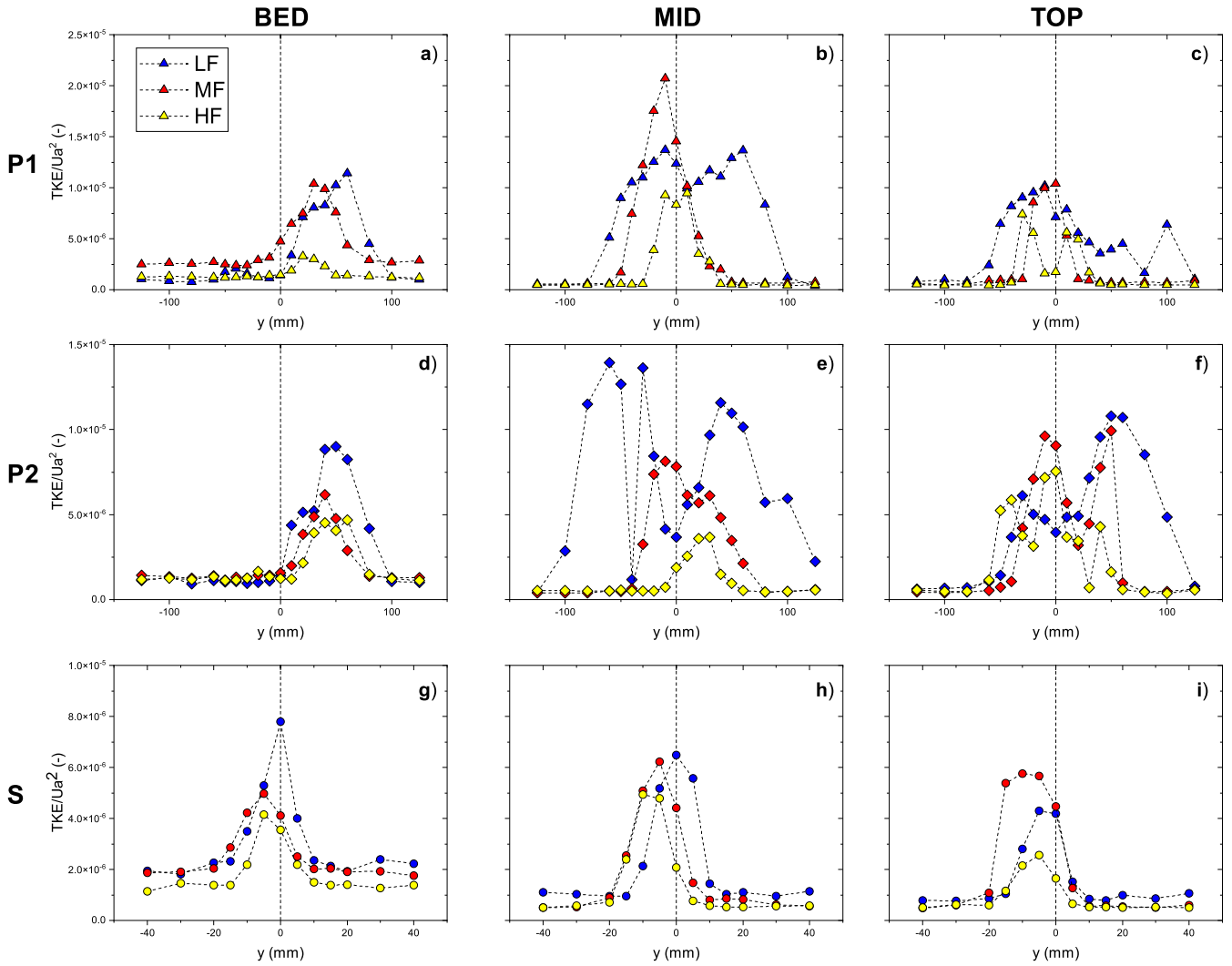

Fig. 13. Turbulent kinetic energy obtained by ADV measurements normalized with the square of ambient velocity. The figures show the profile in the ***y*** direction for all flow conditions, for BED (a,d,g),MID (b,e,h) and TOP (c,f,i) elevations; and for P1 (a,b,c), P2 (d,e,f) and S (g,h,i). The dashed line indicates the position of the plant main stem at the bed.

at each elevation (Figure 7). The difference between $\bar{u}$ and U_a decreased with increasing bulk flow velocity. The normalized velocity decreased on average by 55% for MF condition, and by 20% for HF condition. The observed velocity reduction in the wake region has been associated with sediment deposition downstream of the plant (Bouma et al., 2007).

For $\bar{v}/U_a$ and $\overline{w}/U_a$, the wake width downstream of P1 decreased with increasing bulk flow velocity. The velocity profile of $\bar{v}/U_a$ at BED reversed from positive to negative for all the tested flow conditions (Figure 7d), consistently with the results of Shadaram et al. (2008) gained on a rigid obstruction. However, this trend was less marked at MID and TOP (Figure 7e and Figure 7f). Moreover, for $\bar{v}/U_a$ the magnitude at BED was greater than that observed at MID and TOP. This can be related to the lower heterogeneity of frontal area due to the absence of leaf at BED position.

Figure 7g, Figure 7h and Figure 7i show the normalized averaged vertical velocity $\overline{w}/U_a$ at BED, MID and TOP, respectively. For all the tested flow conditions, $\overline{w}/U_a$ peaked at the lateral position corresponding to the stem of the plant e.g. at the middle of the measured transect ($y = 0$). The results of Elliott et al. (2019) obtained with natural plants of complex morphology showed similar vertical velocity with the maximum magnitude in correspondence of the center of the wake.

Figure 8 reports the dimensionless time averaged velocity ($\bar{u}/U_a$; $\bar{v}/U_a$; $\overline{w}/U_a$) for P2, for all the runs and the investigated transects. The longitudinal profile of normalized streamwise velocity showed a reduction in the wake of plant, consistent with the presence of a "dead zone" downstream of the plant. The decrease in magnitude of $\bar{u}/U_a$ differed along the vertical direction due to heterogeneous distribution of the frontal area of vegetation. Figure 8a, Figure 8b, Figure 8c show the greatest difference between $\bar{u}$ and U_a for the LF condition with the velocity reduction of up to 80%, being particularly marked at MID and TOP (94% and 92%, respectively). The difference between $\bar{u}$ and U_a decreased with increasing bulk flow velocity. The average between the results of three different transects showed the magnitude decreased relative to U_a by up to 47% and 32% at MF and HF, respectively.

The wake width decreased with increasing bulk flow velocity. As measured from the streamwise velocity profile, l_w was on average 124 mm at LF and at HF the wake width decreased until 48 mm.

For $\bar{v}/U_a$ (Figure 8d, Figure 8e, Figure 8f) as for P1, at BED was observed a reversal corresponding to the stem axis that was less notable at MID and TOP. The magnitude of $\bar{v}/U_a$ at BED was greater than at MID and TOP. Figure 8g, Figure 8h and

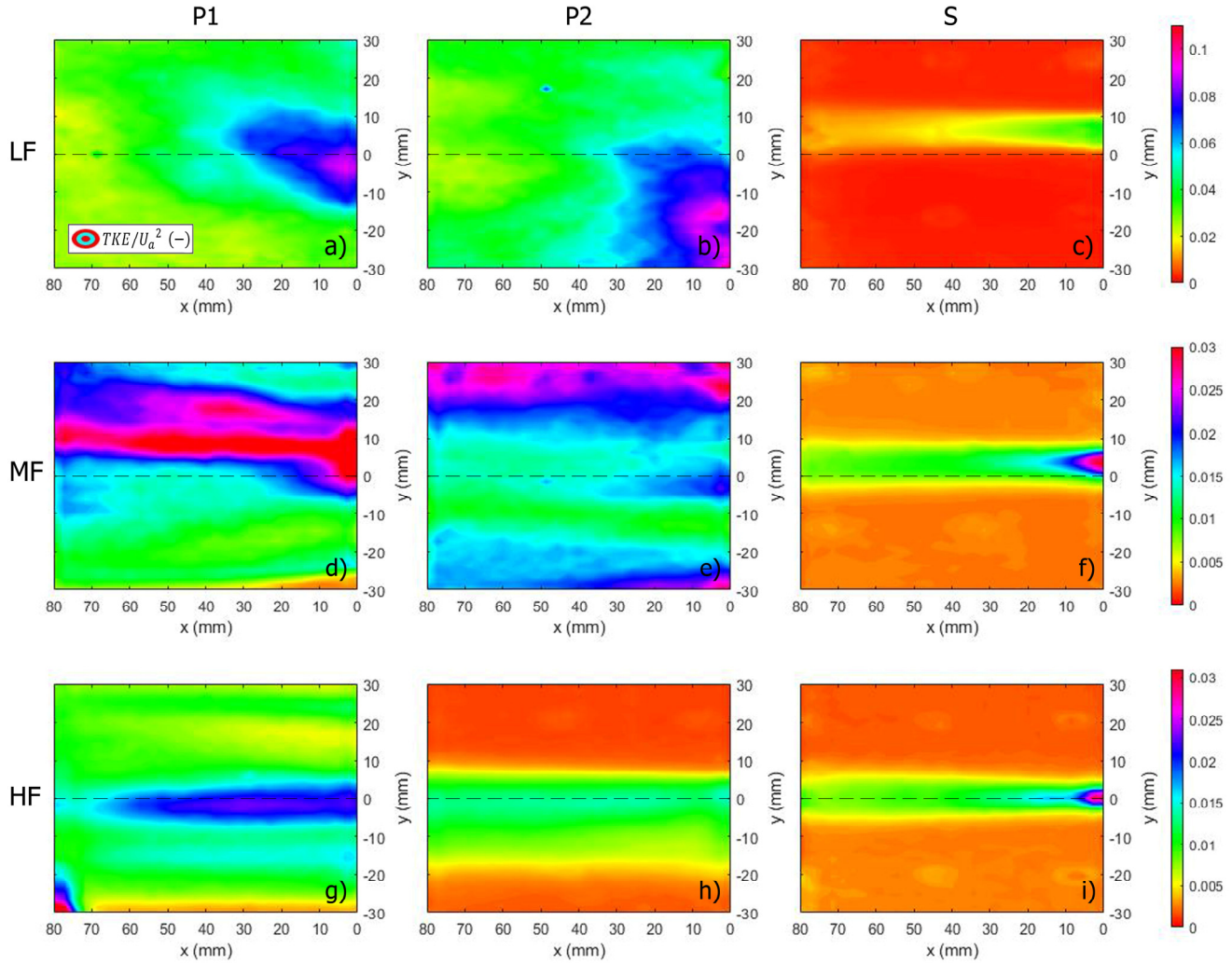

Fig. 14. Turbulent kinetic energy normalized by the square of ambient velocity obtained by PIV measurements at 90 mm from the bottom in a plan of 80 mm x 60 mm, for P1 (a, d, g), P2 (b, e, h) and S (c, f, i); for LF (a, b, c), MF (d, e, f) and HF (g, h, i). Flow direction is from right to left. The dashed line indicates the position of the plant main stem at the bed.

Figure 8i show the lateral profiles of $\overline{w}/U_a$. A strong component in the upward direction corresponding to the stem was observed for MF and HF at MID and TOP measurement positions.

Figure 9 shows the normalized time averaged velocity for all conditions and all transects for the stem. The profiles of the mean streamwise velocity ($\bar{u}/U_a$) were similar to those commonly observed downstream of a rigid obstruction (Shadaram et al., 2008; Wilkerson, 2007). Owing to the homogeneous vertical distribution of the frontal area of the stem, the velocity profiles in the y direction showed similar results for all the measured transects (BED, MID, TOP). The wake width (l_w) downstream of the stem was comparable for all the flow conditions (varying between 8 and 16 mm for HF and MF, respectively) and for all the investigated transects.

Comparing the results of the dimensionless mean velocity at BED position, for all the tested bulk flow velocities, the behavior of P1 and P2 was analogous to that exhibited by the leafless stem. This was ascribed to the absence of leaves at the bottom region since along the first 10 mm from the bed, the plant material consisted only of the stem.

The impact of vegetation reconfiguration on the mean flow field was investigated by comparing the results of normalized streamwise velocity and frontal area of the plants. The Figure 10 shows for all the tested bulk flow velocities and for both plants the results at mid-depth. In particular, the frontal area of vegetation ${A_w}^{(z)}(y)$ was assessed in a 20 mm tall by 10 mm wide rectangle located at the same elevation as the velocity measurement. The computed area ${A_w}^{(mid)}(y)$ was between 80 mm and 100 mm. The local plant frontal area directly influenced the velocity value. Specifically, the regions with higher frontal area were characterized by lower magnitude of $\bar{u}/U_a$. This observation is consistent with previous results (Xu and Nepf, 2020) relating the local mean velocity to the corresponding frontal area of vegetation.

With increasing bulk flow velocity, as shown in Figure 6, the area of the plants decreased, resulting in the profile of $\bar{u}/U_a$ showing a decrease in the wake width. Due to the reconfiguration at HF condition, with the most marked streamlining, the plants' effects on the flow field were similar to those of the leafless stem with a smaller wake width and a smaller decrease in magnitude of normalized mean velocity $\bar{u}$.

Effects of leaves morphology

The effects of the leaves morphology on the flow were investigated by comparing the normalized mean velocity $\bar{u}/U_a$

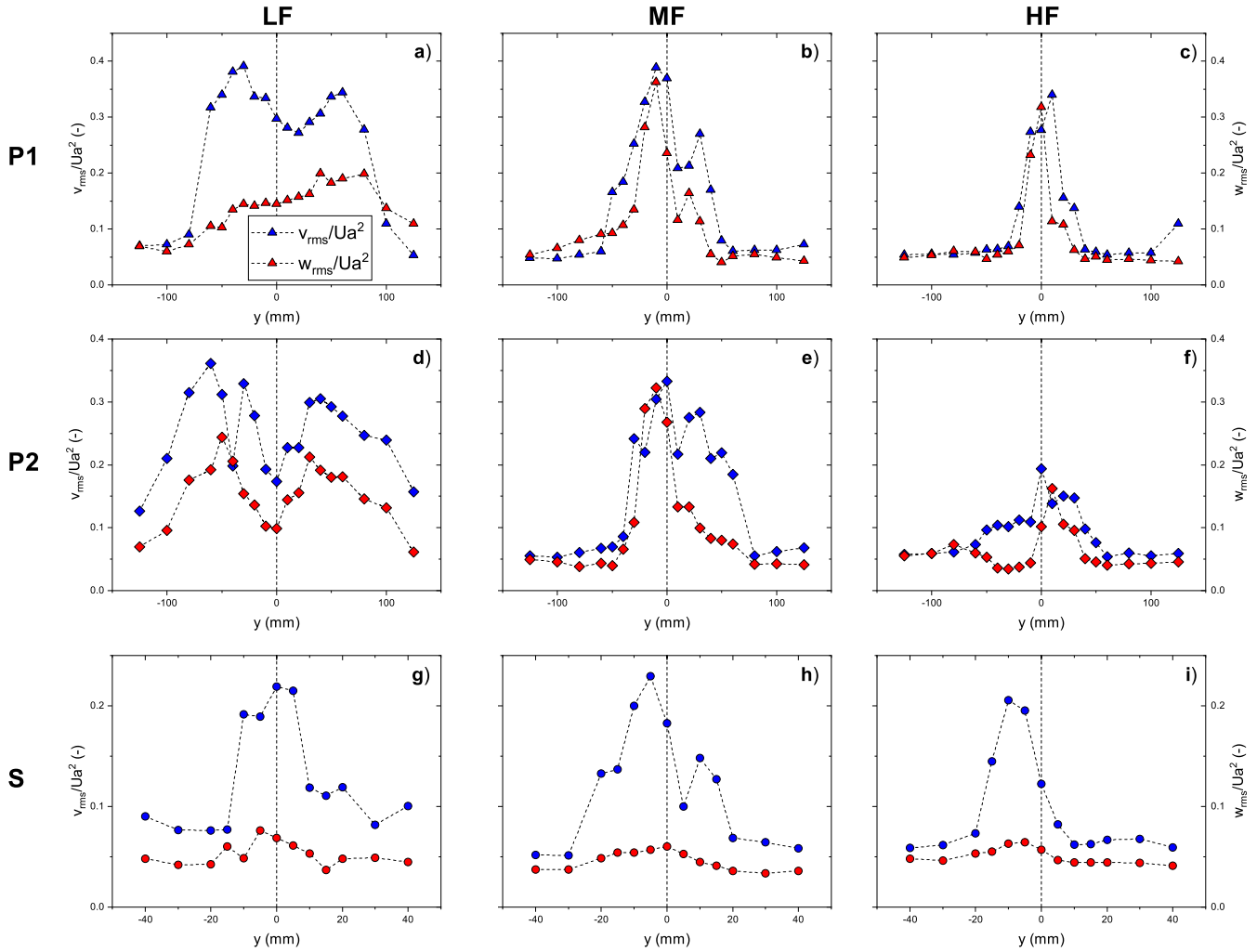

Fig. 15. Root mean square in the $\boldsymbol{y}$ and $\boldsymbol{z}$ direction normalized by the square of ambient velocity. The figures show the profile in the $\boldsymbol{y}$ direction at MID elevation, for LF (a,d,g), MF (b,e,h) and HF (c,f,i); and for P1 (a,b,c), P2 (d,e,f) and S (g,h,i). The dashed line indicates the position of the plant main stem at the bed.

for the plants and the leafless stem. Figure 11 shows the lateral distributions of the streamwise mean velocity as measured with the ADV at MID elevation for P1, P2 and S. Both plants showed similar wake width for the LF condition (127 mm and 124 mm for P1 and P2, respectively). With increasing bulk flow velocity, the difference in l_w between P1 and P2 was more pronounced (at HF 37 mm for P1 and 48 mm for P2), this effect can be ascribed to the different leaf morphology of P1 and P2 plants consistently with the results of Hu et al. (2018). In particular, the study of Hu et al. (2018) showed negligible difference on the total deposition despite the different wake width due to different leaves length. For the leafless stem, no differences in the spatial distribution of $\bar{u}/U_a$ were observed, consistently with the flow features in the wake of a rigid cylinder.

The effect of the morphology of the leaves on the spatial variability of the flow was investigated through PIV measurements. Figure 12 shows the magnitude of normalized mean velocity distribution in the xy plane at mid-depth. For all the tests, the region downstream of the plant was characterized by a velocity reduction in the area of the wake, resembling the canonical plane wake (Tritton, 1977). Consistently with the ADV measurements, the spatial variability of the flow velocity decreased with increasing reconfiguration. At HF condition (Figure 12g and Figure 12h), the wake width exhibited significant reduction for both plants. Indeed, the streamlining of the leaves and the branches in the downstream direction altered the shape of the plant as exposed to the flow. The hydrodynamic effects of the complex morphology due to the presence of leaves and branches were reduced, with the plant resembling a bluff body of more uniform geometry, as testified by the spatial distribution of velocity in the wake. Based on the l_w values from ADV measurements, the spatial distribution of $\bar{u}/U_a$ in the xy plane showed the greatest differences between the two plants at HF. This effect can be associated with the different leaf morphology. Specifically, P2 showed a lower heterogeneity of frontal area at increasing bulk flow velocity with a closer resemblance to the stem than P1. For the leafless stem the flow spatial variability was unaffected by the increasing bulk flow velocity and closely resembled that observed in the wake of a rigid cylinder.

Turbulent flow field

For all the tests, the wake of the plant was a region of high turbulence intensity. A peak in TKE was observed in the wake region, in analogy to the flow downstream of a rigid body.

Figure 13 shows the turbulent kinetic energy normalized by ${U_a}^2$ for all the tests. For P1 and P2, with increasing vegetation

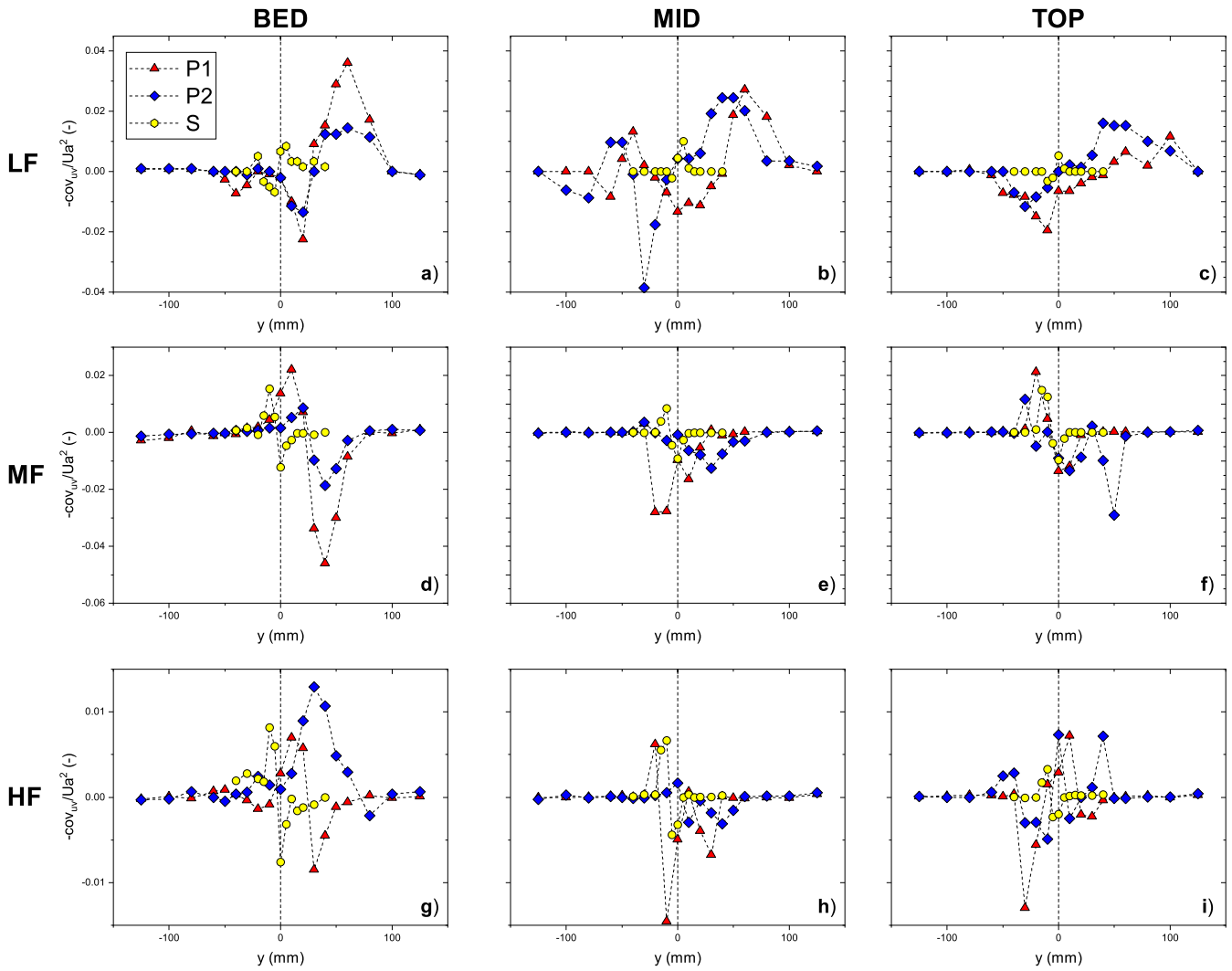

Fig. 16. ***Xy*** component of covariance normalized by the square of ambient velocity. For LF (a,b,c), MF (d,e,f) and HF (g,h,i) and for BED (a,d,g), MID (b,e,h) and TOP (c,f,i) elevations, the figures show the profile in the ***y*** direction downstream of P1,P2 and S. The dashed line indicates the position of the plant main stem at the bed.

reconfiguration, the profile of TKE exhibited a reduction in turbulent wake width. For both plants, l_w^{TKE} was observed to decrease from LF to HF condition, with l_w^{TKE} for P1 and P2 respectively, being on average 160 mm and 164 mm at LF, and 53 mm and 77 mm at HF. Comparing the values of l_w and l_w^{TKE}, the ratio l_w/l_w^{TKE} was similar between P1 and P2 for all the flow conditions, varying between 0.8 at LF and 0.6 at HF.

This result suggests that downstream of a single plant the turbulent flow field is characterized by a greater spatial variability relative to the mean flow. At increasing the bulk flow velocity this difference increased with negligible differences of l_w/l_w^{TKE} between the plants.

Most importantly, the profile of TKE exhibited a decrease in the magnitude of the normalized peaks with increasing U_b. The normalized TKE (Figure 13) showed that for P1 and P2 the peaks at HF were lower than those at LF and MF, with both plants exhibiting the highest magnitude of turbulent kinetic energy at the mid-depth elevation. For both P1 and P2 plants, at LF condition, the maximum *TKE* value decreased from MID to TOP, consistently with previous results obtained on canopies with frontal area increasing with the distance from the bed (Xu and Nepf, 2020).

For all the tests, the TKE downstream of the stem presented a peak coinciding with the stem axis, as observed in the mean flow velocity distributions. For all the elevations (Figure 13g, Figure 13h and Figure 13i), the magnitude of the maximum value decreased with increasing bulk flow velocity. Owing to the reconfiguration and reduction of the frontal projected area at HF condition, P1 and P2 exhibited a behavior similar to that of the leafless stem. Due to absence of leaves at BED position, the TKE profiles were similar between P1, P2 and S for all the tested bulk flow velocities.

The effect of leaves morphology on the spatial variability of the turbulent intensity was further investigated through PIV measurements. Figure 14 reports the magnitude of TKE normalized by ${U_a}^2$ at the mid-depth for all the bulk flow velocities.

In these plots, TKE was computed as $0.5(\overline{u'^2} + \overline{v'^2})$. The results showed the higher magnitude of normalized TKE in correspondence of the wake of the plant with the maximum in correspondence of the stem axis ($y = 0$), consistently with Elliott et al. (2019). This can be ascribed to the velocity gradient generating the von Kármán vortex along the center of the wake enhancing the turbulent intensity. Reconfiguration influenced the spatial distribution of TKE. Consistently with the ADV measurements, for P1 and P2 a high spatial variability

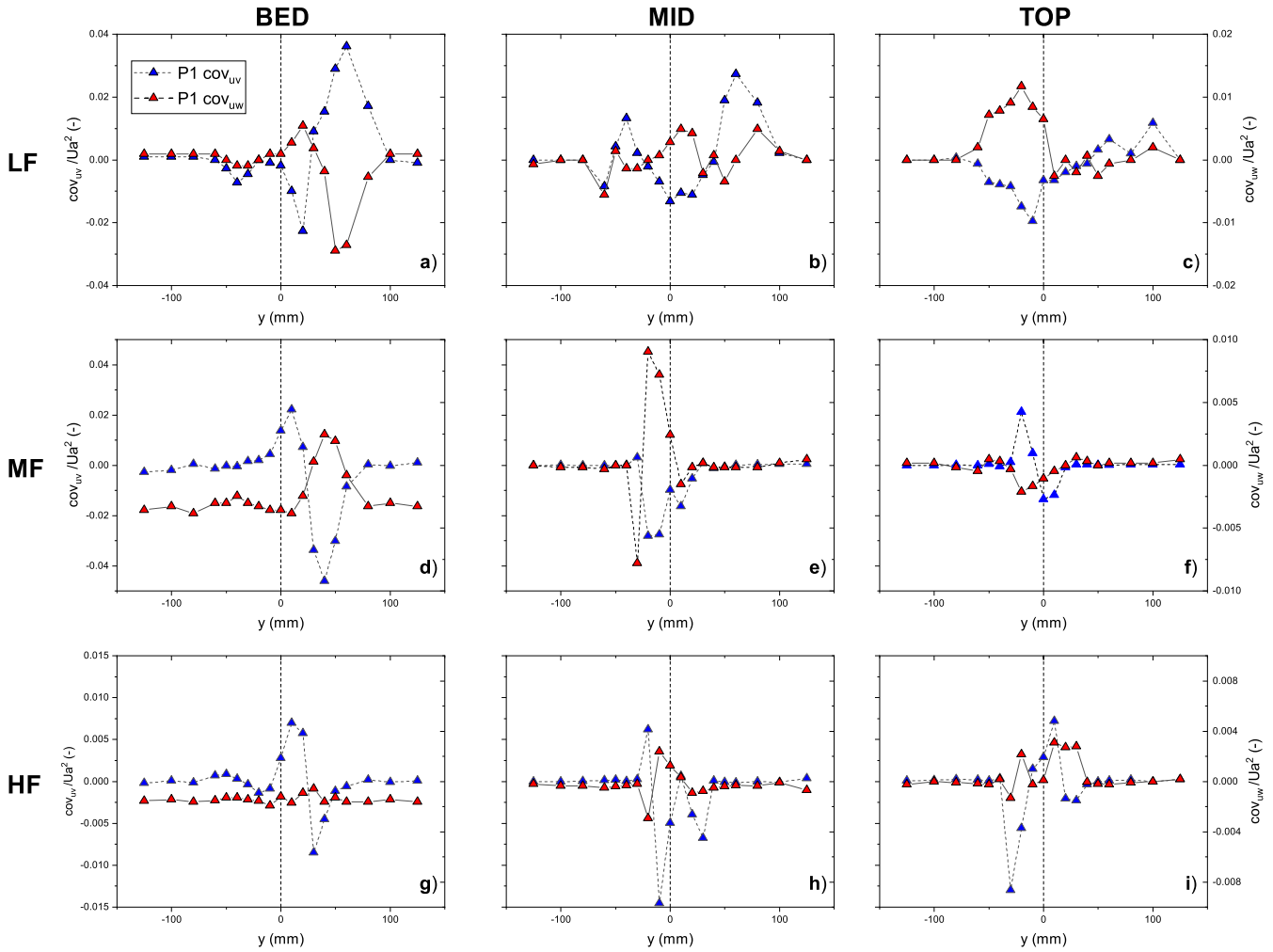

Fig. 17. Xy and xz components of covariance normalized by the square of ambient velocity. For LF (a,b,c), MF (d,e,f) and HF (g,h,i), and for BED (a,d,g), MID (b,e,h) and TOP (c,f,i) elevations, the figures show the profile in the y direction downstream of P1. The dashed line indicates the position of the plant main stem at the bed.

was noted at LF and MF, with leaf morphology presenting a more marked effect at the highest U_b. At HF, the turbulent flow field downstream of the plants (Figure 14g and Figure 14h) resembled that in the wake of the leafless stem (Figure 14i). In particular, the longer leaves of plant P2 streamlined better to the flow, resulting in lower variability of frontal projected area. As a consequence, the TKE downstream of P2 more closely resembled that downstream of the stem than P1.

The spatial variability of the turbulent intensity generated downstream of the stem was not affected by the variation of the bulk flow velocity. With increasing U_b, the turbulent wake width showed no significant variation.

In Figure 15 the lateral distributions of the root mean square of the fluctuating velocity at mid-depth for the plants and the leafless stem are shown. Downstream of P1 and P2 the lateral distributions of v_{rms} and w_{rms} were comparable for MF and HF conditions. By contrast, at LF condition, the turbulent intensity in the y direction showed higher magnitude respect to that in the z direction for both plants. This was consistent with the results of Yagci et al. (2010) who described the influence of a single emergent plant on the kinetic energy, noting a difference in the magnitude between the lateral and vertical components.

Downstream of the stem, lower turbulent intensity was observed in comparison with the P1 and P2 plants (Figure 15g, Figure 15h and Figure 15i). For the leafless stem, the magnitude of v_{rms} was greater than that of w_{rms} for all bulk flow velocity, differently from the results gained on P1 and P2. This difference can be ascribed to the different hydrodynamic behavior of natural foliated vegetation. Indeed, this observation is in agreement with the results of Caroppi et al. (2021b) and Tanino and Nepf (2007) obtained with rigid cylinder, for which the magnitude of w_{rms} can be neglected respect to v_{rms}. At HF condition, due to reconfiguration, the lateral profile of v_{rms} showed similar results between the plants and leafless stem.

The xy component of the Reynold stress (cov_{uv}) normalized by the square of U_a is reported in Figure 16 for all the tests. Owing to the complex morphology of the plants, the lateral profile of Reynold stress showed marked spatial variability.

When the plant reconfiguration increased, the magnitude of the normalized cov_{uv} decreased and a smaller spatial variability was observed. For the leafless cases, for which the frontal area was constant at each transect with no reconfiguration, the cov_{uv} profile showed no appreciable differences between the different U_b. In particular, the lateral distributions of Reynolds stress downstream of the stem resembled that observed downstream of a rigid cylinder. Indeed, in agreement with Wygnanski et al. (1986) the profile of the Reynold stress reverse from positive to negative in correspondence of the center of the wake ($y = 0$).

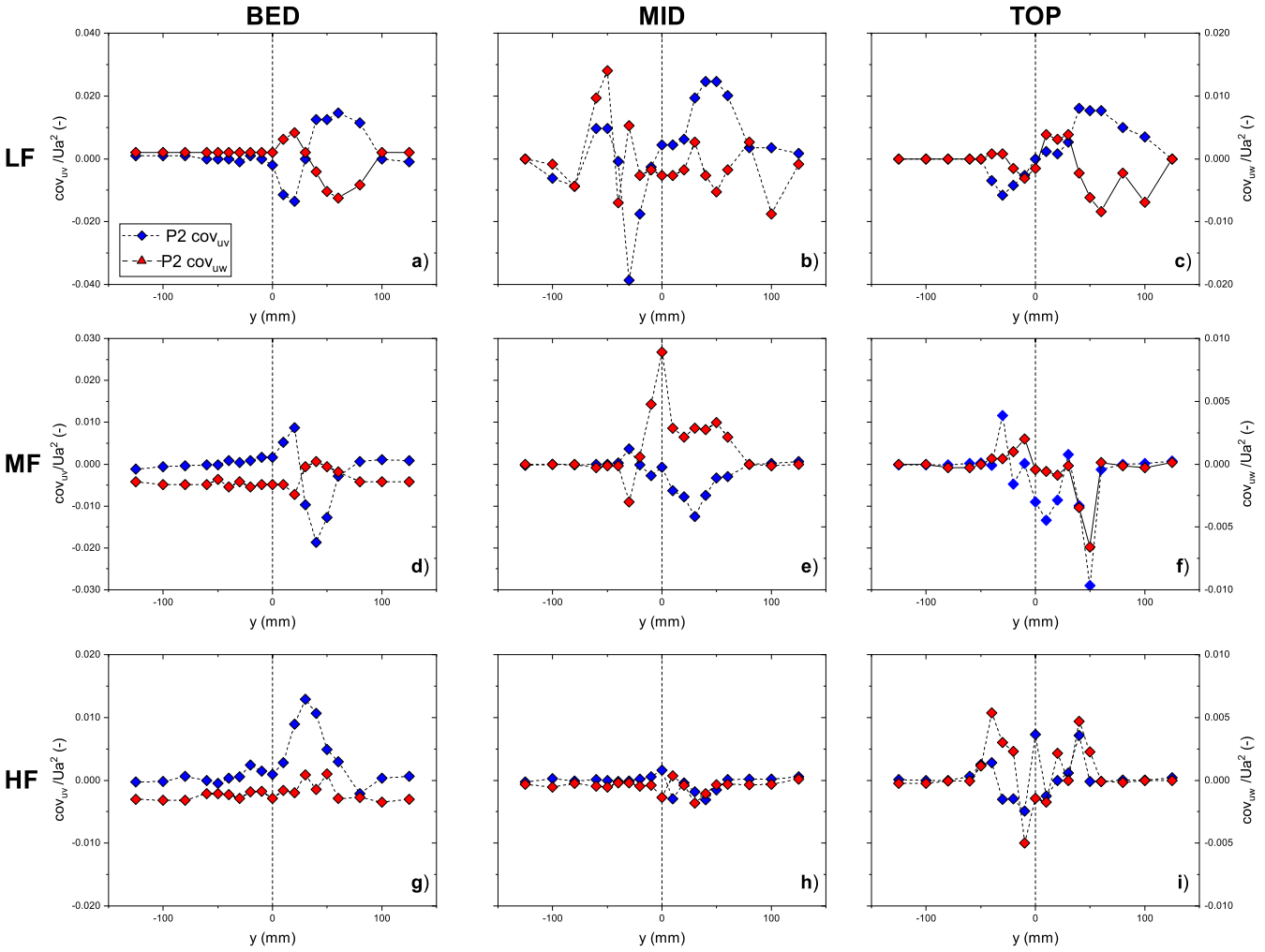

Fig. 18. Xy and xz components of covariance normalized by the square of ambient velocity. For LF (a,b,c), MF (d,e,f) and HF (g,h,i), and for BED (a,d,g), MID (b,e,h) and TOP (c,f,i) elevations, the figures show the profile in the y direction downstream of P2. The dashed line indicates the position of the plant main stem at the bed.

Figure 17 and Figure 18 show the comparison between the xy and xz components of the Reynolds stress for all flow conditions for P1 and P2, respectively. The lateral distributions of cov_{uv} and cov_{uw} were approximately symmetrical about the x axis. However, the magnitude of cov_{uv} was larger than that of cov_{uw}, indicating the presence of stronger velocity gradients in the lateral direction (y) rather than the vertical direction (z).

This result suggests that in presence of isolated plants occupying the whole water column, the exchange of momentum in the lateral direction is improved relative to that occurring in the vertical direction. This can be ascribed to the higher variability of the frontal area of plants in the lateral direction relative to that in the z direction. Increasing bulk flow velocity resulted in the distribution being progressively less symmetrical, with decrease in the magnitude of the Reynolds stresses.

CONCLUDING REMARKS

This paper investigates the flow-vegetation interaction at the scale of an isolated, flexible foliated plant. Two plants with the same total frontal area and with leaves of different morphologies were tested under different bulk flow velocities to investigate the hydrodynamic impacts of plant reconfiguration and leaf morphology on the flow. The effects of seasonal variability of vegetation on the flow structure were explored through experiments with the leafless stem. Plant reconfiguration induced the frontal projected area to decrease by up to the 80% of the undeformed value in dry conditions. Under increasing bulk flow velocity, the plants exhibited stem bending and streamlining of leaves. By contrast, in leafless conditions, negligible differences in the frontal area were observed, with the stem exhibiting a rigid behavior.

This study highlighted the influence of the spatial distribution of vegetation frontal area on the mean flow field. For all the investigated bulk flow velocities, the lateral distribution of the mean velocity measured downstream of the leafless stem was comparable to that downstream of a rigid cylinder. In all the tests, the lateral profiles of the normalized mean velocity showed a decrease in the velocity magnitude in the wake of the plant, with the wake width decreasing with increasing bulk flow velocity due to the vegetation reconfiguration.

The reconfiguration of the flexible foliated plants influenced the turbulent flow field. The magnitude of the turbulent kinetic energy and the turbulent wake width decreased with increasing bulk flow velocity, owing to the increasing reconfiguration and the decrease in plant frontal projected area. For the stem, the turbulent flow field was comparable to that downstream of a rigid cylinder.

The PIV measurements were mainly used to analyze the effects of the different morphology of the leaves on the flow.

For the mean and turbulent flow field, small differences were observed between the plants under low and medium bulk flow velocities. At high bulk flow velocity condition, the wake width and the turbulent wake width were different for P1 and P2 plants. The plant with elongated leaves exhibited a behavior closer to that of the leafless stem for the highest bulk flow velocities.

In conclusion, our results indicate that the complex structural properties of woody plants, resulting from the presence of leaves, stems and branches, govern the flow features at the scale of the single plant and at the scale of the plant subparts. The local effects on the flow are profoundly affected by flexibility-induced reconfiguration, that can markedly alter the spatial distribution of the flow properties and the magnitude of the turbulent kinetic energy, with implications on the momentum and mass transport processes.

Acknowledgements. The authors gratefully acknowledge the laboratory technicians Antonio Fusco and Domenico Palmiero for their help in arranging the experiments.

REFERENCES

Aberle, J., Järvelä, J., 2013. Flow resistance of emergent rigid and flexible floodplain vegetation. Journal of Hydraulic Research, 51, 1, 33–45. https://doi.org/10.1080/00221686.2012.754795

Ackerman, J.D., Okubo, A., Okubot, A., 1993. Reduced Mixing in a Marine Macrophyte Canopy. Functional Ecology, 7, 3, 305–309.

Biggs, H.J., Nikora, V.I., Gibbins, C.N., Cameron, S.M., Papadopoulos, K., Stewart, M., Fraser, S., Vettori, D., Savio, M., O'Hare, M.T., Kucher, M., Hicks, D.M., 2019. Flow interactions with an aquatic macrophyte: a field study using stereoscopic particle image velocimetry. Journal of Ecohydraulics, 4, 2, 113–130. https://doi.org/10.1080/24705357.2019.1606677

Boothroyd, R.J., Hardy, R.J., Warburton, J., Marjoribanks, T.I., 2017. Modeling complex flow structures and drag around a submerged plant of varied posture. Water Resources Research, 53, 4, 2877–2901. https://doi.org/10.1002/2016WR020186

Bouma, T.J., van Duren, L.A., Temmerman, S., Claverie, T., Blanco-Garcia, A., Ysebaert, T., Herman, P.M.J., 2007. Spatial flow and sedimentation patterns within patches of epibenthic structures: Combining field, flume and modelling experiments. Continental Shelf Research, 27, 8, 1020–1045. https://doi.org/10.1016/j.csr.2005.12.019

Box, W., Västilä, K., Järvelä, J., 2019. The interplay between flow field, suspended sediment concentration, and net deposition in a channel with flexible bank vegetation. Water, 11, 11. https://doi.org/10.3390/w11112250

Caroppi, G., Gualtieri, P., Fontana, N., Giugni, M., 2020. Effects of vegetation density on shear layer in partly vegetated channels. Journal of Hydro-Environment Research, 30, 82–90. https://doi.org/10.1016/j.jher.2020.01.008

Caroppi, G., Järvelä, J., 2022. Shear layer over floodplain vegetation with a view on bending and streamlining effects. Environmental Fluid Mechanics, 22, 587–618. https://doi.org/10.1007/s10652-022-09841-w

Caroppi, G., Västilä, K., Järvelä, J., Rowiński, P.M., Giugni, M., 2019. Turbulence at water-vegetation interface in open channel flow: Experiments with natural-like plants. Advances in Water Resources, 127, 180–191. https://doi.org/10.1016/j.advwatres.2019.03.013

Caroppi, G., Västilä, K., Gualtieri, P., Järvelä, J., Giugni, M., Rowiński, P.M., 2021. Comparison of flexible and rigid vegetation induced shear layers in partly vegetated channels. Water Resources Research, 57, 3. https://doi.org/10.1029/2020WR028243

Caroppi, G., Västilä, K., Järvelä, J., Lee, C., Ji, U., Kim, H.S., Kim, S., 2022. Flow and wake characteristics associated with riparian vegetation patches: Results from field-scale experiments. Hydrological Processes, 36, 2. https://doi.org/10.1002/hyp.14506

Chen, Z., Ortiz, A., Zong, L., Nepf, H., 2012. The wake structure behind a porous obstruction and its implications for deposition near a finite patch of emergent vegetation. Water Resources Research, 48, 9. https://doi.org/10.1029/2012WR012224

Elliott, S.H., Tullos, D.D., Walter, C., 2019. Physical modeling of the feedbacks between a patch of flexible Reed Canarygrass (*Phalaris arundinacea*), wake hydraulics, and downstream deposition. Environmental Fluid Mechanics, 19, 1, 255–277. https://doi.org/10.1007/s10652-018-9622-8

Gurnell, A., 2015. Plants as river system engineers: Further comments. Earth Surface Processes and Landforms, 40, 1, 135–137. https://doi.org/10.1002/esp.3671

Harder, D.L., Speck, O., Hurd, C.L., Speck, T., 2004. Reconfiguration as a prerequisite for survival in highly unstable flow-dominated habitats. Journal of Plant Growth Regulation, 23, 2, 98–107. https://doi.org/10.1007/s00344-004-0043-1

Hu, Z., Lei, J., Liu, C., Nepf, H., 2018. Wake structure and sediment deposition behind models of submerged vegetation with and without flexible leaves. Advances in Water Resources, 118, 28–38. https://doi.org/10.1016/j.advwatres.2018.06.001

Jalonen, J., Järvelä, J., 2014. Estimation of drag forces caused by natural woody vegetation of different scales. Journal of Hydrodynamics, 26, 4, 608–623. https://doi.org/10.1016/S1001-6058(14)60068-8

Järvelä, J., 2005. Effect of submerged flexible vegetation on flow structure and resistance. Journal of Hydrology, 307, 1–4, 233–241. https://doi.org/10.1016/j.jhydrol.2004.10.013

Jesson, M.A., Bridgeman, J., Sterling, M., 2015. Novel software developments for the automated post-processing of high volumes of velocity time-series. Advances in Engineering Software, 89, 36–42. https://doi.org/10.1016/j.advengsoft.2015.06.007

Jesson, M., Sterling, M., Bridgeman, J., 2013. Despiking velocity time-series-Optimisation through the combination of spike detection and replacementmethods. Flow Measurement and Instrumentation, 30, 45–51. https://doi.org/10.1016/j.flowmeasinst.2013.01.007

King, A.T., Tinoco, R.O., Cowen, E.A., 2012. A k-ε turbulence model based on the scales of vertical shear and stem wakes valid for emergent and submerged vegetated flows. Journal of Fluid Mechanics, 701, 1–39. https://doi.org/10.1017/jfm.2012.113

Kubrak, E., Kubrak, J., Rowiński, P.M., 2008. Vertical velocity distributions through and above submerged, flexible vegetation. Hydrological Sciences Journal, 53, 4, 905–920. https://doi.org/10.1623/hysj.53.4.905

Lee, J.K., Roig, L.C., Jenter, H.L., Visser, H.M., 2004. Drag coefficients for modeling flow through emergent vegetation in the Florida Everglades. Ecological Engineering, 22, 4–5, 237–248.

Łoboda, A.M., Bialik, R.J., Karpiński, M., Przyborowski, Ł., 2018. Seasonal changes in the biomechanical properties of *Elodea canadensis* Michx. Aquatic Botany, 147, 43–51. https://doi.org/10.1016/j.aquabot.2018.03.006

Łoboda, A.M., Karpiński, M., Bialik, R.J., 2018. On the relationship between aquatic plant stem characteristics and drag force: Is a modeling application possible? Water, 10, 5. https://doi.org/10.3390/w10050540

Miler, O., Albayrak, I., Nikora, V., O'Hare, M., 2012. Biome-

chanical properties of aquatic plants and their effects on plant-flow interactions in streams and rivers. Aquatic Sciences, 74, 1, 31–44. https://doi.org/10.1007/s00027-011-0188-5

Mossa, M., Ben Meftah, M., De Serio, F., Nepf, H.M., 2017. How vegetation in flows modifies the turbulent mixing and spreading of jets. Scientific Reports, 7, 1, 1–14. https://doi.org/10.1038/s41598-017-05881-1

Nepf, H.M., Mugnier, C.G., Zavistoski, R.A., 1997. The effects of vegetation on longitudinal dispersion. Estuarine, Coastal and Shelf Science, 44, 6, 675–684.

Nikora, V., 2010. Hydrodynamics of Aquatic Ecosystems: An interface between ecology, biomechanics and environmental fluid mechanics. River Research and Applications, 26, 4, 367–384. https://doi.org/10.1002/rra.1291

Nikora, V., Larned, S., Nikora, N., Debnath, K., Cooper, G., Reid, M., 2008. Hydraulic resistance due to aquatic vegetation in small streams: field study. Journal of Hydraulic Engineering, 134, 9, 1326–1332.

Nikora, V., Cameron, S., Albayrak, I., Miler, O., Nikora, N., Siniscalchi, F., Stewart, M., O'Hare, M., Rodi, W., 2012. Flow-biota interactions in aquatic systems: scales, mechanisms, and challenges. In: Rodi, W., Uhlmann, M. (Eds.): Environmental Fluid Mechanics: Memorial Volume in Honour of Professor Gerhard H. Jirka. IAHR Monographs, Chapter 11.

Nikora, V.I., Pearson, C.P., Shankar, U., 1999. Scaling properties in landscape patterns: New Zealand experience. Landscape Ecology, 14, 17–33.

Poggi, D., Krug, C., Katul, G.G., 2009. Hydraulic resistance of submerged rigid vegetation derived from first-order closure models. Water Resources Research, 45, 10, 1–14. https://doi.org/10.1029/2008WR007373

Proust, S., Fernandes, J.N., Leal, J.B., Rivière, N., Peltier, Y., 2017. Mixing layer and coherent structures in compound channel flows: Effects of transverse flow, velocity ratio, and vertical confinement. Water Resources Research, 53, 4, 3387–3406. https://doi.org/10.1002/2016WR019873

Przyborowski, Ł., Łoboda, A.M., Bialik, R.J., Västilä, K., 2019. Flow field downstream of individual aquatic plants—Experiments in a natural river with *Potamogeton crispus* L. and *Myriophyllum spicatum* L. Hydrological Processes, 33, 9, 1324–1337. https://doi.org/10.1002/hyp.13403

Pugliese, F., Caroppi, G., Zingraff-Hamed, A., Lupp, G., Gerundo, C., 2022. Assessment of NBSs effectiveness for flood risk management: The Isar River case study. Journal of Water Supply: Research and Technology-Aqua, 71, 1, 42–61. https://doi.org/10.2166/aqua.2021.101

Puijalon, S., Bouma, T.J., Douady, C.J., van Groenendael, J., Anten, N.P.R., Martel, E., Bornette, G., 2011. Plant resistance to mechanical stress: Evidence of an avoidance-tolerance trade-off. New Phytologist, 191, 4, 1141–1149. https://doi.org/10.1111/j.1469-8137.2011.03763.x

Rowiński, P.M., Västilä, K., Aberle, J., Järvelä, J., Kalinowska, M.B., 2018. How vegetation can aid in coping with river management challenges: A brief review. Ecohydrology and Hydrobiology, 18, 4, 345–354. https://doi.org/10.1016/j.ecohyd.2018.07.003

Shadaram, A., Fard, A., Rostamy, N., 2008. Experimental study of near wake flow behind a rectangular cylinder. American Journal of Applied Sciences, 5, 8, 917–926.

Siniscalchi, F., Nikora, V., 2013. Dynamic reconfiguration of aquatic plants and its interrelations with upstream turbulence and drag forces. Journal of Hydraulic Research, 51, 1, 46–55. https://doi.org/10.1080/00221686.2012.743486

Stoesser, T., Kim, S.J., Diplas, P., 2010. Turbulent flow through idealized emergent vegetation. Journal of Hydraulic Engineering, 136, 12, 1003–1017. https://doi.org/10.1061/(asce)hy.1943-7900.0000153

Stone, B.M., Shen, H.T., 2002. Hydraulic resistance of flow in channels with cylindrical roughness. Journal of Hydraulic Engineering, 128, 5, 500–506. https://doi.org/10.1061/(asce)0733-9429(2002)128:5(500)

Sukhodolova, T.A., Sukhodolov, A.N., 2012. Vegetated mixing layer around a finite-size patch of submerged plants: 1. Theory and field experiments. Water Resources Research, 48, 10. https://doi.org/10.1029/2011WR011804

Tabacchi, E., Lambs, L., Guilloy, H., Planty-Tabacchi, A.-M., Muller, E., Décamps, H., 2000. Impacts of riparian vegetation on hydrological processes. Hydrol. Process., 14, 2959–2976.

Tanino, Y., Nepf, H.M., 2007. Experimental investigation of lateral dispersion in aquatic canopies. In: Proc. 32nd Congress of IAHR.

Tanino, Y., Nepf, H.M., 2008. Laboratory investigation of mean drag in a random array of rigid, emergent cylinders. Journal of Hydraulic Engineering, 134, 1, 34–41. https://doi.org/10.1061/(asce)0733-9429(2008)134:1(34)

Termini, D., 2015. Flexible vegetation behaviour and effects on flow conveyance: experimental observations. International Journal of River Basin Management, 13, 4, 401–411. https://doi.org/10.1080/15715124.2015.1012519

Tinoco, R.O., Coco, G., 2016. A laboratory study on sediment resuspension within arrays of rigid cylinders. Advances in Water Resources, 92, 1–9. https://doi.org/10.1016/j.advwatres.2016.04.003

Tritton, D.J., 1977. Physical Fluid Dynamics. Springer Netherlands. https://doi.org/10.1007/978-94-009-9992-3

Västilä, K., Järvelä, J., 2014. Modeling the flow resistance of woody vegetation using physically based properties of the foliage and stem. Water Resources Research, 50, 1, 229–245. https://doi.org/10.1002/2013WR013819

Vogel, S., 1989. Drag and reconfiguration of broad leaves in high winds. Journal of Experimental Botany, 40, 8, 941–948. https://doi.org/10.1093/jxb/40.8.941

Weissteiner, C., Jalonen, J., Järvelä, J., Rauch, H.P., 2015. Spatial-structural properties of woody riparian vegetation with a view to reconfiguration under hydrodynamic loading. Ecological Engineering, 85, 85–94. https://doi.org/10.1016/j.ecoleng.2015.09.053

White, B.L., Nepf, H.M., 2008. A vortex-based model of velocity and shear stress in a partially vegetated shallow channel. Water Resources Research, 44, 1. https://doi.org/10.1029/2006WR005651

Whittaker, P., Wilson, C.A.M.E., Aberle, J., 2015. An improved Cauchy number approach for predicting the drag and reconfiguration of flexible vegetation. Advances in Water Resources, 83, 28–35. https://doi.org/10.1016/j.advwatres.2015.05.005

Wilkerson, G.V., 2007. Flow through trapezoidal and rectangular channels with rigid cylinders. Journal of Hydraulic Engineering, 133, 5, 521–533.

Wygnanski, I., Champagne, A.N.F., Marasli, D.B., 1986. On the large-scale structures in two-dimensional, small-deficit, turbulent wakes. Journal of Fluid Mechanics, 168, 31–71. https://doi.org/10.1017/S0022112086000289

Xu, Y., Nepf, H., 2020. Measured and predicted turbulent kinetic energy in flow through emergent vegetation with real plant morphology. Water Resources Research, 56, 12, 1–20. https://doi.org/10.1029/2020WR027892

Yagci, O., Tschiesche, U., Kabdasli, M.S., 2010. The role of different forms of natural riparian vegetation

on turbulence and kinetic energy characteristics. Advances in Water Resources, 33, 5, 601–614. https://doi.org/10.1016/j.advwatres.2010.03.008

Yagci, O., Celik, M.F., Kitsikoudis, V., Ozgur Kirca, V.S., Hodoglu, C., Valyrakis, M., Duran, Z., Kaya, S., 2016. Scour patterns around isolated vegetation elements. Advances in Water Resources, 97, 251–265. https://doi.org/10.1016/j.advwatres.2016.10.002

Yager, E.M., Schmeeckle, M.W., 2013. The influence of vegetation on turbulence and bed load transport. Journal of Geophysical Research: Earth Surface, 118, 3, 1585–1601. https://doi.org/10.1002/jgrf.20085

Zong, L., Nepf, H., 2012. Vortex development behind a finite porous obstruction in a channel. Journal of Fluid Mechanics, 691, 368–391. https://doi.org/10.1017/jfm.2011.479

Received 18 November 2021
Accepted 9 June 2022